Determination of the non-ideal response of a high temperature tokamak plasma to a static external magnetic perturbation via asymptotic matching

Richard Fitzpatrick

Citation: Physics of Plasmas **24**, 072506 (2017); doi: 10.1063/1.4990701
View online: http://dx.doi.org/10.1063/1.4990701
View Table of Contents: http://aip.scitation.org/toc/php/24/7
Published by the American Institute of Physics

Determination of the non-ideal response of a high temperature tokamak plasma to a static external magnetic perturbation via asymptotic matching

Richard Fitzpatrick
Department of Physics, Institute for Fusion Studies, University of Texas at Austin, Austin, Texas 78712, USA

(Received 31 March 2017; accepted 16 June 2017; published online 6 July 2017)

Asymptotic matching techniques are used to calculate the response of a high temperature tokamak plasma with a realistic equilibrium to an externally generated, non-axisymmetric, static, magnetic perturbation. The plasma is divided into two regions. In the outer region, which comprises most of the plasma, the response is governed by the linearized equations of marginally stable, ideal-magnetohydrodynamics (MHD). In the inner region, which is strongly localized around the various rational surfaces within the plasma (where the marginally stable, ideal-MHD equations become singular), the response is governed by Glasser-Greene-Johnson linear layer physics. For the sake of simplicity, the paper focuses on the situation where the plasma at one of the internal rational surfaces is locked to the external perturbation, whereas that at the other surfaces is rotating. *Published by AIP Publishing.* [http://dx.doi.org/10.1063/1.4990701]

I. INTRODUCTION

Tokamak plasmas are highly sensitive to externally generated, non-axisymmetric, static, magnetic perturbations. Such perturbations, which are conventionally termed "error-fields," are present in all tokamak experiments because of imperfections in magnetic field-coils. An error-field can drive magnetic reconnection in an otherwise tearing-stable plasma, giving rise to the formation of "locked" (i.e., non-rotating) magnetic island chains on so-called "rational" magnetic flux-surfaces within the plasma.[1] Such chains, which are generally known as "locked modes," severely degrade global energy confinement[2] and often trigger major disruptions.[3–5] Tokamak plasmas are particularly vulnerable to locked modes in their low-β startup phases[3–8] and also as they approach the ideal β-limit.[9–11]

The response of a tokamak plasma to an externally generated, non-axisymmetric, static, magnetic perturbation is generally very different to that predicted by naively superimposing the vacuum perturbation onto the equilibrium magnetic field. A major cause of this difference is the excitation of shielding currents at the various rational surfaces within the plasma. These currents act to suppress driven magnetic reconnection and must be overcome before significant locked mode formation can occur.[1,12] Shielding currents are excited by plasma rotation[1] or by a combination of pressure gradients and the characteristic favorable average magnetic field-line curvature present in tokamak plasmas.[13] The latter mechanism for exciting shielding currents is of particular significance for ITER,[14] because of the low intrinsic plasma rotation expected in this device. In addition to shielding currents at rational surfaces, an external magnetic perturbation excites currents that are distributed throughout the bulk of the plasma. In a tokamak equilibrium with a realistic aspect-ratio, boundary shape, and pressure, these currents profoundly modify the perturbation.[15] Consequently, cylindrical models, or models that rely on large aspect-ratio, low-β, orderings (all of which do a very poor job of modeling the distributed currents), are unable to accurately predict the response of a realistic tokamak equilibrium to a static magnetic perturbation and often give highly misleading results.[15]

There are three main approaches to accurately modeling the response of a realistic tokamak equilibrium to a externally generated, non-axisymmetric, static, magnetic perturbation. The first approach involves solving the equations of resistive magnetohydrodynamics (resistive-MHD) throughout the whole plasma.[16,17] Unfortunately, this approach is both time-consuming and highly inefficient—basically, because inertial and resistive effects are only important in the immediate vicinities of the various rational surfaces within the plasma, and the response of the bulk of the plasma to the external perturbation is governed by the equations of marginally stable, ideal magnetohydrodynamics (ideal-MHD), which are much simpler than the full resistive-MHD equations. The second approach is to solve the marginally stable, ideal-MHD equations throughout the whole plasma, placing ideal current sheets at the rational surfaces.[18] Such an approach facilitates very rapid calculations, but is of limited accuracy, because it neglects any non-ideal response of the plasma to the external perturbation at the rational surfaces, and this response is often crucially important. The final approach is to solve the linearized, marginally stable, ideal-MHD equations throughout the bulk of the plasma and asymptotically match the solutions thus obtained to non-ideal layer (or magnetic island) solutions at the rational surfaces.[19–24] This approach, which is much more efficient than the first, and is able to capture the non-ideal effects neglected in the second, is the one adopted in this paper.

II. HOMOGENEOUS TEARING/TWISTING DISPERSION RELATION

Consider a tokamak plasma surrounded by a vacuum region that is bounded by a perfectly conducting wall. In the following, all lengths are normalized to the major radius of the plasma magnetic axis, R_0, all magnetic field-strengths to the vacuum toroidal field-strength at the magnetic axis, B_0, and all plasma pressures to B_0^2/μ_0. We employ a

right-handed flux coordinate system, r, θ, ϕ. Here, r is a flux-surface label with dimensions of length which is such that $r=0$ at the magnetic axis, $r=b>0$ at the plasma boundary, and $r=a>b$ at the wall. Thus, the vacuum corresponds to the region $b<r<a$. Moreover, θ is a "straight" poloidal angle defined such that $\theta=0$ on the inboard midplane. Finally, ϕ is the geometric toroidal angle. The Jacobian of the coordinate system is (see Appendix A 1)

$$(\nabla r\times\nabla\theta\cdot\nabla\phi)^{-1}=r\,R^2. \tag{1}$$

(Here, R, ϕ, Z is a conventional right-handed cylindrical coordinate system whose symmetry axis corresponds to the toroidal symmetry axis of the plasma.) The equilibrium magnetic field is written as (see Appendix A 2)

$$\mathbf{B}(r,\theta)=\frac{r\,g}{q}\,\nabla(\phi-q\,\theta)\times\nabla r, \tag{2}$$

where $q(r)$ is the safety-factor profile and $g(r)/R$ is the toroidal magnetic field-strength.

Consider a global, non-axisymmetric, resistive instability whose toroidal mode number is $n>0$. As is well known, the determination of global resistive stability in a high temperature tokamak plasma can be reduced to an asymptotic matching problem.[25] The system is conveniently divided into two regions. In the "outer" region, which comprises most of the plasma, the perturbation is described by the linearized, marginally stable (i.e., zero inertia), equations of ideal-MHD. However, these equations become singular on rational magnetic flux-surfaces. In the "inner" region, which is strongly localized around the various rational surfaces, non-ideal effects such as resistivity and inertia become important. The solution in the vicinity of a given rational surface can be separated into tearing and twisting (i.e., interchange) parity components.[26] The two parities are completely independent of one another in the various segments of the inner region but are coupled together in the surrounding outer region. Finally, simultaneous asymptotic matching of the layer solutions in the inner region to the ideal-MHD solution in the outer region yields a matrix tearing/twisting dispersion relation.[19–24,27,28]

Let the m_j, for $j=1,J$, be the coupled poloidal harmonics included in the stability calculation. The linearized, marginally stable, ideal-MHD equations that govern the perturbation in the outer region become singular at the various rational surfaces lying within the plasma. These surfaces satisfy $q(r_k)=m_k/n$, for $k=1,K$, where $0<r_k<b$, and m_k is one of the m_j. Writing

$$\delta\mathbf{B}\cdot\nabla r=\mathrm{i}\sum_{j=1,J}\frac{\psi_j(r)}{r\,R^2}\,\exp\left[\mathrm{i}\,(m_j\,\theta-n\,\phi)\right], \tag{3}$$

where $\delta\mathbf{B}$ is the perturbed magnetic field, the general analytic solution of the linearized, marginally stable, ideal-MHD equations in the immediate vicinity of the kth rational surface is such that (see Appendix A 5)

$$\psi_k(r)=\Psi_k^{\pm}\,F_k\,|x_k|^{\nu_{Lk}}+\Delta\Psi_k^{\pm}\,F_k\,\mathrm{sgn}(x_k)\,|x_k|^{\nu_{Sk}}+A_k\,x_k+\cdots, \tag{4}$$

where

$$x_k=\left(\frac{r-r_k}{r_k}\right), \tag{5}$$

$$F_k=\left(\frac{m_k^2\,\langle|\nabla r|^{-2}\rangle+n^2\,r^2}{2\,\sqrt{-D_{Ik}}}\right)^{1/2}_{r_k}, \tag{6}$$

and $\nu_{Lk}=1/2-\sqrt{-D_{Ik}}$, $\nu_{Sk}=1/2+\sqrt{-D_{Ik}}$. Here, $\langle\cdots\rangle=\oint(\cdots)\,d\theta/2\pi$ is a flux-surface average operator, and

$$D_{Ik}=\frac{r\,P'}{f^2\,s^2}\left\{\left(\langle|\nabla r|^{-2}\rangle+\frac{r^2}{q^2}\right)\left[-f\,\frac{d}{dr}\left(\frac{r}{f}\,\langle R^2\rangle\right)+\frac{r\,P'}{f^2}\,\langle|\nabla r|^{-2}\,R^4\rangle\right]-\frac{r\,P'}{f^2}\,\langle|\nabla r|^{-2}\,R^2\rangle^2+s\,\langle|\nabla r|^{-2}\,R^2\rangle\right\}_{r_k}-\frac{1}{4}, \tag{7}$$

a standard ideal interchange stability parameter evaluated at the surface.[26] Moreover, $f(r)=r\,g/q$, $P(r)$ is the plasma pressure profile, $s(r)=r\,q'/q$, and $'\equiv d/dr$. The plus superscript refers to the region $x_k>0$, whereas the minus superscript refers to the region $x_k<0$. It is helpful to define (see Appendix A 5)

$$\Psi_k^e=\frac{1}{2}\left(\Psi_k^+ +\Psi_k^-\right), \tag{8}$$

$$\Psi_k^o=\frac{1}{2}\left(\Psi_k^+ -\Psi_k^-\right), \tag{9}$$

$$\Delta\Psi_k^e=\Delta\Psi_k^+ +\Delta\Psi_k^-, \tag{10}$$

$$\Delta\Psi_k^o=\Delta\Psi_k^+ -\Delta\Psi_k^-. \tag{11}$$

The complex quantities Ψ_k^e and Ψ_k^o parameterize the amount of magnetic reconnection generated by tearing- and twisting-parity modes, respectively, at the kth rational surface. (Thus, in a completely ideal plasma, $\Psi_k^e=\Psi_k^o=0$, for all k.) Moreover, the complex quantities

$$\Delta_k^e=\frac{\Delta\Psi_k^e}{\Psi_k^e}, \tag{12}$$

$$\Delta_k^o=\frac{\Delta\Psi_k^o}{\Psi_k^o}, \tag{13}$$

are completely determined by the tearing- and twisting-parity resistive layer solutions, respectively, in the vicinity of the kth rational surface.[26]

The linearized, marginally stable, ideal-MHD equations can be solved numerically in the outer region (via adaptive-step integration), subject to the constraint that the solution is well behaved at the magnetic axis, and satisfies the physical boundary condition $\delta\mathbf{B}\cdot\nabla r=0$ at $r=a$. Simultaneous asymptotic matching of this numerical solution to the analytic solution (4) at every rational surface in the plasma yields the homogeneous tearing/twisting dispersion relation (see Appendix A 7)

$$\sum_{k'=1,K}\left[\left(E_{kk'}^e-\delta_{kk'}\,\Delta_{k'}^e\right)\Psi_{k'}^e+\Gamma_{kk'}\,\Psi_{k'}^o\right]=0, \tag{14}$$

$$\sum_{k'=1,K}\left[\left(E^o_{kk'}-\delta_{kk'}\,\Delta^o_{k'}\right)\Psi^o_{k'}+\Gamma'_{kk'}\,\Psi^e_{k'}\right]=0, \tag{15}$$

for $k=1,K$. Here, the elements of the $\mathbf{E}^e$, $\mathbf{E}^o$, $\mathbf{\Gamma}$, and $\mathbf{\Gamma}'$ matrices only depend on the ideal-MHD solution in the outer region. On the other hand, the Δ^e_k and Δ^o_k values depend on the non-ideal layer solutions in the various segments of the inner region. In particular, the elements of the $\mathbf{E}^e$, $\mathbf{E}^o$, $\mathbf{\Gamma}$, and $\mathbf{\Gamma}'$ matrices are independent of the complex growth-rate, γ, of the instability, whereas the Δ^e_k and Δ^o_k values are generally functions of γ. Finally, the elements of the $\mathbf{E}^e$, $\mathbf{E}^o$, $\mathbf{\Gamma}$, and $\mathbf{\Gamma}'$ matrices satisfy the important symmetry constraints (see Appendix A 7)

$$E^e_{kk'}=E^{e*}_{k'k}, \tag{16}$$

$$E^o_{kk'}=E^{o*}_{k'k}, \tag{17}$$

$$\Gamma'_{kk'}=\Gamma^*_{k'k} \tag{18}$$

for $k,k'=1,K$.

It is easily demonstrated that zero net toroidal electromagnetic torque is exerted on the plasma in the outer region as a consequence of tearing or twisting perturbations[21] (see Appendix A 4). On the other hand, the net torque exerted on the segment of the inner region centered on the kth rational surface is (see Appendix A 5)

$$\delta T_k=2\,n\,\pi^2\left[\mathrm{Im}\left(\Delta^e_k\right)|\Psi^e_k|^2+\mathrm{Im}\left(\Delta^o_k\right)|\Psi^o_k|^2\right]. \tag{19}$$

It follows from Eqs. (14)–(18) that

$$\sum_{k=1,K}\delta T_k=0. \tag{20}$$

In other words, zero net toroidal electromagnetic torque is exerted on the plasma as a whole.

III. INHOMOGENEOUS TEARING/TWISTING DISPERSION RELATION

Suppose that the perfectly conducting wall at $r=a$ is subject to a small amplitude, non-axisymmetric, static, displacement

$$\boldsymbol{\xi}^x=\frac{\delta r\,\nabla r}{|\nabla r|^2}, \tag{21}$$

where

$$\delta r(\theta,\phi)=\Xi(\theta)\,\exp\left(-\mathrm{i}\,n\,\phi\right)=\sum_{j=1,J}\Xi_j\,\exp\left[\mathrm{i}\left(m_j\,\theta-n\,\phi\right)\right]. \tag{22}$$

Thus, the displaced wall is located at

$$r=a+\delta r(\theta,\phi). \tag{23}$$

The response of the plasma to the static magnetic perturbation generated by the wall displacement is governed by the inhomogeneous tearing/twisting dispersion relation, which takes the form (see Appendix A 8)

$$\sum_{k'=1,K}\left[\left(E^e_{kk'}-\delta_{kk'}\,\Delta^e_{k'}\right)\Psi^e_{k'}+\Gamma_{kk'}\,\Psi^o_{k'}\right]=\chi^e_k, \tag{24}$$

$$\sum_{k'=1,K}\left[\left(E^o_{kk'}-\delta_{kk'}\,\Delta^o_{k'}\right)\Psi^o_{k'}+\Gamma'_{kk'}\,\Psi^e_{k'}\right]=\chi^o_k, \tag{25}$$

for $k=1,K$. Here,

$$\chi^{e,o}_k=\langle\,\xi^{e,o*}_k(\theta)\,\Xi(\theta)\,\rangle=\sum_{j=1,J}\xi^{e,o*}_{k,j}\,\Xi_j, \tag{26}$$

where

$$\xi^{e,o}_k(\theta)=\sum_{j=1,J}\xi^{e,o}_{k,j}\,\exp\left(\mathrm{i}\,m_j\,\theta\right). \tag{27}$$

As explained in Appendix A 8, the $\xi^{e,o}_{k,j}$ can be calculated from the homogeneous tearing/twisting solutions introduced in Sec. II. Finally, the net toroidal electromagnetic torque exerted by the external perturbation on the segment of the inner region centered on the kth rational surface is (see Appendix A 8)

$$\delta T^x_k=-2\,n\,\pi^2\,\mathrm{Im}\left(\Psi^{e*}_k\,\chi^e_k+\Psi^{o*}_k\,\chi^o_k\right). \tag{28}$$

IV. LINEAR LAYER RESPONSE MODEL

We can make no further progress without adopting a particular model that describes the non-ideal physics governing the segments of the inner region centered on the various rational surfaces within the plasma. Suppose that each segment is governed by Glasser-Greene-Johnson linear resistive-MHD layer physics.[26] This model is particularly appropriate to cases in which the plasma is stable to tearing/twisting instabilities, and there is strong shielding of the plasma interior from the external magnetic perturbation (i.e., the external perturbation drives very little magnetic reconnection within the plasma, and, hence, the plasma response at the various rational surfaces is accurately modeled by the linear theory).

Let $\rho(r)$, $\eta(r)$, and $\Omega_\phi(r)$ be the plasma mass density, electrical resistivity, and toroidal angular velocity profiles, respectively. The functions

$$\omega_A(r)=\frac{B_0}{R_0}\,\frac{1}{\sqrt{\mu_0\,\rho(r)}}, \tag{29}$$

$$\omega_R(r)=\frac{\eta(r)}{\mu_0\,R_0^2\,\bar{a}^2}, \tag{30}$$

$$S(r)=\frac{\omega_A}{\omega_R}, \tag{31}$$

where $\bar{a}$ is the wall minor radius (see Sec. V), are the shear-Alfvén frequency, the resistive diffusion rate, and the Lundquist number profiles, respectively. According to the Glasser-Greene-Johnson resistive layer theory, we can write (see Appendix B)

$$\Delta^{e,o}_k=(S_k)^{\mu_k}\,\tilde{\Delta}^{e,o}_k\left(\tilde{Q}_k=-\mathrm{i}\,n\,\tilde{\Omega}_k\right), \tag{32}$$

where

$$\tilde{\Omega}_k = \frac{\Omega_k}{\omega_{Ak}^{2/3}\,\omega_{Rk}^{1/3}}, \tag{33}$$

and $\mu_k = (2/3)\sqrt{-D_{Ik}}$, $S_k = S(r_k)$, $\Omega_k = \Omega_\phi(r_k)$, $\omega_{Ak} = \omega_A(r_k)$, $\omega_{Rk} = \omega_R(r_k)$. (Here, we have assumed that $\gamma = 0$, because we are dealing with the response of a tearing/twisting stable plasma to a static magnetic perturbation.) Note that the normalized layer quantities $\tilde{\Delta}_k^{e,o}$, which are determined via numerical solution of the Glasser-Greene-Johnson layer equations,[29] are independent of the local Lundquist numbers, S_k.

V. PLASMA EQUILIBRIUM

The unperturbed location of the perfectly conducting wall surrounding the plasma is written parametrically as

$$R = R_c[1 + \bar{a}\,\cos(\omega + \bar{\delta}\,\sin\omega)], \tag{34}$$

$$Z = R_c\,\bar{a}\,\kappa\,\sin\omega \tag{35}$$

for $0 \le \omega \le 2\pi$. Here, $\bar{a}$ is the wall minor radius, κ the elongation, and $\bar{\delta}$ the triangularity. The parameter R_c is automatically adjusted to ensure that the plasma magnetic axis lies at $R = 1$. The chosen equilibrium profiles are

$$\frac{dP}{d\Psi} = P_0\begin{cases}(1 - s^2/s_b^2) & 0 < s < s_b\\ 0 & s_b \le s \le 1,\end{cases} \tag{36}$$

and

$$I^*(\Psi) = I_0\begin{cases}(1 - s^2/s_b^2)^\nu & 0 < s < s_b\\ 0 & s_b \le s \le 1,\end{cases} \tag{37}$$

where

$$s = \sqrt{1 - \frac{\Psi}{\Psi_0}}, \tag{38}$$

$$s_b = \sqrt{1 - \frac{\Psi_b}{\Psi_0}}, \tag{39}$$

and $0 < s_b < 1$. Here, $P(\Psi)$ is the plasma pressure profile,

$$I^*(\Psi) = -\frac{\langle R^2\rangle}{\langle R\rangle}\frac{dP}{d\Psi} - \frac{1}{\langle R\rangle}\,g\,\frac{dg}{d\Psi}, \tag{40}$$

the flux-surface averaged toroidal current density,

$$\Psi(r) = -\int_r^a \frac{r\,g}{q}\,dr \tag{41}$$

the poloidal magnetic flux, and $\Psi_0 \equiv \Psi(0)$, $\Psi_b \equiv \Psi(b)$. Note that $\Psi(a) = 0$. The parameter I_0 is adjusted such that the central safety-factor, $q_0 \equiv q(0)$, takes a particular value. The parameter ν is adjusted such that the edge safety-factor, $q_b \equiv q(b)$, takes a particular value. Finally, the parameter P_0 is adjusted such that the normal beta,

$$\beta_N = \frac{\beta(\%)\,\bar{a}(\mathrm{m})\,B_0(\mathrm{T})}{I_p(\mathrm{MA})}, \tag{42}$$

takes a particular value. Here, the total toroidal current, I_p, and total plasma beta, β, are defined in Ref. 30.

VI. EXAMPLE CALCULATION

A. Example equilibrium

Consider an example plasma equilibrium for which the parameters $\bar{a}$, κ, and $\bar{\delta}$ are given the JET-like values 0.3, 1.8, and 0.25, respectively.[31] The chosen values of the central safety factor, the edge safety factor, and the normal beta are $q_0 = 1.05$, $q_b = 3.95$, and $\beta_N = 0.25$, respectively. Finally, the boundary parameter s_b is given the value 0.95. It follows that $a = 0.4057$ and $b = 0.3557$. Furthermore, there are two $n = 1$ rational surfaces in the plasma: the $q = 2$ (or $k = 1$) surface at $r/b = 0.7284$ and the $q = 3$ (or $k = 2$) surface at $r/b = 0.9075$. The equilibrium magnetic flux-surfaces, as well as the location of the wall and the plasma boundary, are shown in Fig. 1. The safety-factor profile is shown in Fig. 2. (The equilibrium is calculated using the CHEASE code.[30])

B. Calculation of $n = 1$ shielding factors

The inhomogeneous tearing/twisting dispersion relation (24) and (25) can be written in the general form [see Eq. (32)]

$$\sum_{k'=1,K}\left(\left[E^e_{kk'} - \delta_{kk'}\,(S_{k'})^{\mu_{k'}}\,\tilde{\Delta}^e_{k'}\right]\Psi^e_{k'} + \Gamma_{kk'}\,\Psi^o_{k'}\right) = \chi^e_k, \tag{43}$$

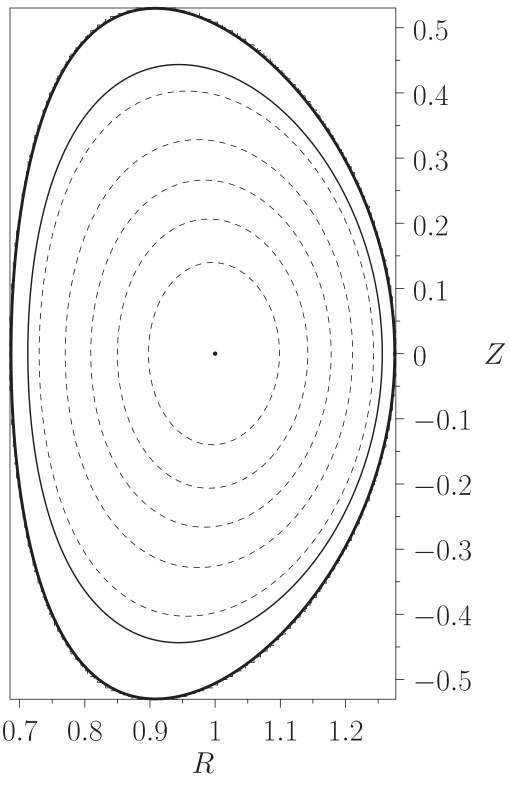

FIG. 1. Unperturbed magnetic flux-surfaces for a plasma equilibrium characterized by $\bar{a} = 0.3$, $\kappa = 1.8$, $\bar{\delta} = 0.25$, $s_b = 0.95$, $q_0 = 1.05$, $q_b = 3.95$, and $\beta_N = 0.25$. The thick solid curve shows the location of the perfectly conducting wall surrounding the plasma, the thin solid curve shows the location of the plasma boundary, and the dashed curves show magnetic flux-surfaces inside the plasma.

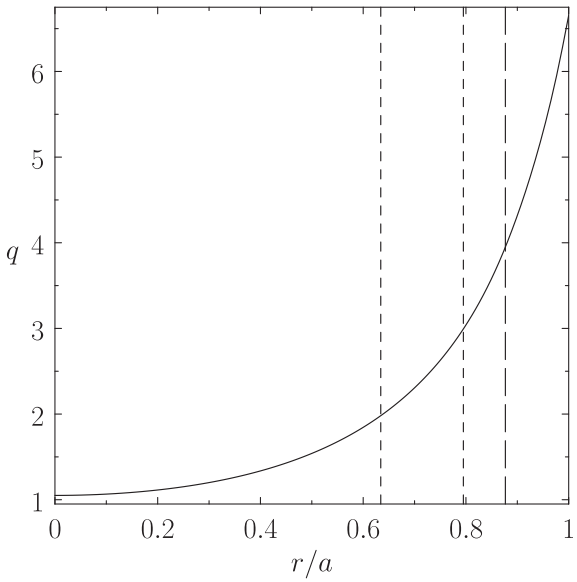

FIG. 2. Safety-factor profile for a plasma equilibrium characterized by $\bar{a} = 0.3$, $\kappa = 1.8$, $\bar{\delta} = 0.25$, $s_b = 0.95$, $q_0 = 1.05$, $q_b = 3.95$, and $\beta_N = 0.25$. The long-dashed vertical line indicates the location of the plasma boundary. The two short-dashed vertical lines indicate the locations of the $q = 2$ and $q = 3$ surfaces.

$$\sum_{k'=1,K} \left(\left[E^o_{kk'} - \delta_{kk'} \, (S_{k'})^{\mu_{k'}} \, \tilde{\Delta}^o_{k'} \right] \Psi^o_{k'} + \Gamma'_{kk'} \, \Psi^e_{k'} \right) = \chi^o_k, \quad (44)$$

for $k = 1, K$. In a high temperature tokamak plasma, the Lundquist numbers, S_k, are typically very much greater than unity and also much greater than the $|E^{e,o}_{kk'}|$, $|\Gamma_{kk'}|$, $|\Gamma'_{kk'}|$, and $|\tilde{\Delta}^{e,o}_k|$. It follows that the external perturbation drives negligible magnetic reconnection inside the plasma (i.e., the $|\Psi^{e,o}_k|$ are very much less than the $|\chi^{e,o}_k|$), except when one, or more, of the $|\tilde{\Delta}^e_k|$ or the $|\tilde{\Delta}^o_k|$ is small compared to unity.

Figures 3 and 4 show the variation of the $n = 1$ twisting- and tearing-parity layer response functions at the $q = 2$ surface—$\tilde{\Delta}^o_1$ and $\tilde{\Delta}^e_1$, respectively—with the normalized local plasma toroidal angular velocity, $\tilde{\Omega}_1$, calculated (via the finite-difference method described in Ref. 29) for the example plasma equilibrium illustrated in Figs. 1 and 2. The variation of the corresponding response functions at the $q = 3$ surface with the local toroidal angular velocity is analogous.

It can be seen, from Fig. 3, that the magnitude of the twisting-parity response function, $\tilde{\Delta}^o_1$, is always much greater than unity. This turns out to be a general result. Thus, we deduce that, in general, $|\tilde{\Delta}^o_k| \gg 1$ for $k = 1, K$. This implies, from (44), that the Ψ^o_k are all negligibly small: i.e., the twisting-parity responses of the various segments of the inner region to the external perturbation are negligible. In this situation, the inhomogeneous dispersion relation, (43) and (44), simplifies to give

$$\sum_{k'=1,K} \left[E^e_{kk'} - \delta_{kk'} \, (S_{k'})^{\mu_{k'}} \, \tilde{\Delta}^e_{k'} \right] \Psi^e_{k'} \simeq \chi^e_k, \quad (45)$$

for $k = 1, K$.

It can be seen, from Fig. 4, that the magnitude of the tearing-parity response function, $\tilde{\Delta}^e_1$, is small compared to unity when the magnitude of the normalized local toroidal angular velocity, $\tilde{\Omega}_1$, is of order unity. On the other hand,

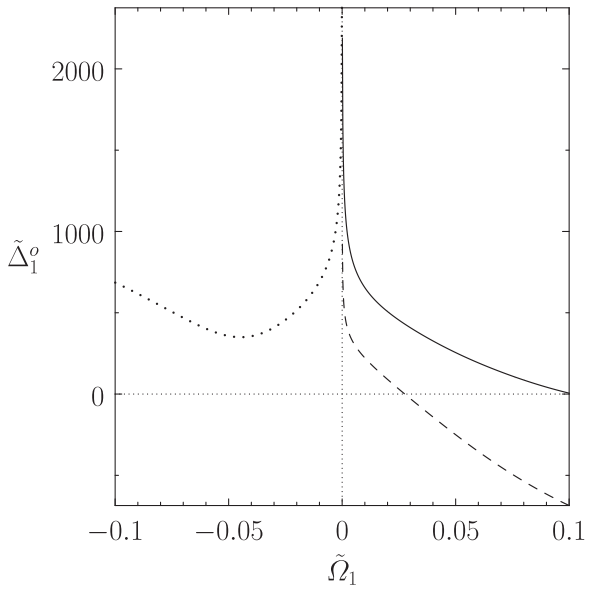

FIG. 3. Variation of the $n = 1$ twisting-parity layer response function at the $q = 2$ surface, $\tilde{\Delta}^o_1$, with the normalized local plasma toroidal angular velocity, $\tilde{\Omega}_1$, for a plasma equilibrium characterized by $\bar{a} = 0.3$, $\kappa = 1.8$, $\bar{\delta} = 0.25$, $s_b = 0.95$, $q_0 = 1.05$, $q_b = 3.95$, and $\beta_N = 0.25$. The solid and dashed curves on the right-hand side show $\mathrm{Re}(\tilde{\Delta}^o_1)$ and $\mathrm{Im}(\tilde{\Delta}^o_1)$, respectively. The dotted curve on the left-hand side shows $|\tilde{\Delta}^o_1|$. Note that $\mathrm{Re}(\tilde{\Delta}^o_1)$ and $\mathrm{Im}(\tilde{\Delta}^o_1)$ are even and odd functions of $\tilde{\Omega}_1$, respectively.

$|\tilde{\Delta}^e_1| \gg 1$ when $|\tilde{\Omega}_1| \gg 1$. This also turns out to be a general result. Thus, we deduce that, in general, $|\tilde{\Delta}^e_k| \gg 1$ when $|\tilde{\Omega}_k| \gg 1$, for $k = 1, K$. This implies, from (45), that Ψ^e_k is negligibly small when $|\tilde{\Omega}_k| \gg 1$. In the following, for the sake of simplicity, we shall suppose that the plasma toroidal angular velocity profile is sufficiently sheared that only one

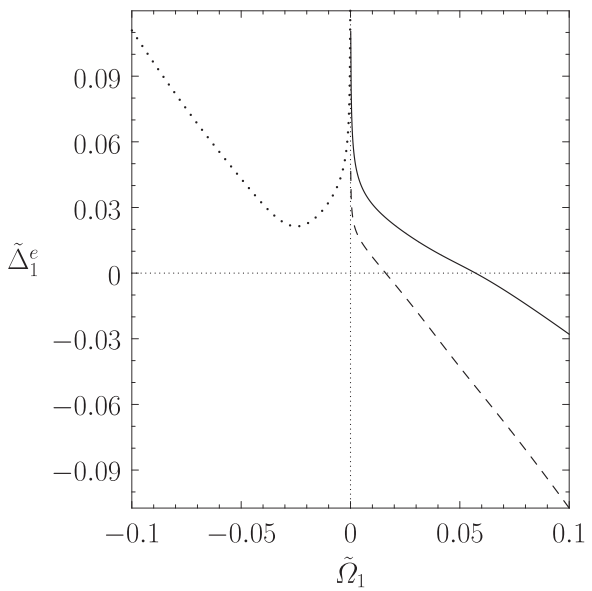

FIG. 4. Variation of the $n = 1$ tearing-parity layer response function at the $q = 2$ surface, $\tilde{\Delta}^e_1$, with the normalized local plasma toroidal angular velocity, $\tilde{\Omega}_1$, for a plasma equilibrium characterized by $\bar{a} = 0.3$, $\kappa = 1.8$, $\bar{\delta} = 0.25$, $s_b = 0.95$, $q_0 = 1.05$, $q_b = 3.95$, and $\beta_N = 0.25$. The solid and dashed curves on the right-hand side show $\mathrm{Re}(\tilde{\Delta}^e_1)$ and $\mathrm{Im}(\tilde{\Delta}^e_1)$, respectively. The dotted curve on the left-hand side shows $|\tilde{\Delta}^e_1|$. Note that $\mathrm{Re}(\tilde{\Delta}^e_1)$ and $\mathrm{Im}(\tilde{\Delta}^e_1)$ are even and odd functions of $\tilde{\Omega}_1$, respectively.

of the $|\tilde{\Omega}_k|$ is comparable with unity, and the others are all much greater than unity. Let the surface in question be the kth surface. Thus, $\Psi^e_{k'\neq k}=0$, and the inhomogeneous dispersion relation (45) further simplifies to give

$$\Psi^e_k \simeq \frac{\chi^e_k}{E^e_{kk}-(S_k)^{\mu_k}\,\tilde{\Delta}^e_k}. \tag{46}$$

According to Eq. (28), the toroidal electromagnetic torque exerted by the external perturbation on the plasma in the immediate vicinity of the kth rational surface takes the form

$$\delta T^x_k \simeq 2\,n\,\pi^2\,\frac{(S_k)^{\mu_k}\,\mathrm{Im}\left(\tilde{\Delta}^e_k\right)\,|\chi^e_k|^2}{|E^e_{kk}-(S_k)^{\mu_k}\,\tilde{\Delta}^e_k|^2}. \tag{47}$$

It is evident, from Fig. 4, that this torque acts to adjust the local toroidal angular velocity, $\tilde{\Omega}_k$, such that $\mathrm{Im}(\tilde{\Delta}^e_k)=0$, at which point $|\tilde{\Delta}^e_k|$ attains a minimum value: i.e., the shielding of the kth rational surface from the external perturbation is minimized. Let us suppose that this process, which we shall term the "locking" of the kth rational surface to the external perturbation, has taken place. Let $\tilde{\Omega}_{kc}$ be the critical local normalized toroidal angular velocity at which $\mathrm{Im}(\tilde{\Delta}^e_k)=0$, and let $\tilde{\Delta}^e_{kc}$ be the corresponding value of $\tilde{\Delta}^e_k$. Note that $\tilde{\Delta}^e_{kc}$ is real and positive.

Suppose that the tearing-parity mode that only reconnects magnetic flux at the kth rational surface is intrinsically unstable: i.e., $E^e_{kk}>0$. [Here, we are assuming that the plasma toroidal angular velocity profile is sufficiently sheared that if $\tilde{Q}_k\equiv\tilde{\gamma}_k-\mathrm{i}\,n\,\tilde{\Omega}_k$ is of order unity for the kth rational surface then $|\tilde{Q}_{k'}|\gg 1$ for all $k'\neq k$, where $\tilde{\gamma}_k=\gamma/\left[\omega^{2/3}_{Ak}\,\omega^{1/3}_{Rk}\right]$, and γ is the complex growth-rate. Under these circumstances, the coupled homogenous tearing mode dispersion relation factorizes into approximately independent dispersion relations for modes that only reconnect magnetic flux at a single rational surface in the plasma. The mode that reconnects flux at the kth rational surface is unstable when $E^e_{kk}>0$, and vice versa.[21]] In this situation, Eq. (46) becomes

$$\Psi^e_k \simeq -\frac{\chi^e_k}{|E^e_{kk}|}\,\Sigma_k(S_k), \tag{48}$$

where

$$\Sigma_k(S_k)=\frac{1}{(S_k/S_{kc})^{\mu_k}-1}, \tag{49}$$

and

$$S_{kc}=\left(\frac{|E^e_{kk}|}{\tilde{\Delta}^e_{kc}}\right)^{1/\mu_k} \tag{50}$$

is the critical local Lundquist number above which the mode in question is stabilized by the Glasser effect (i.e., by the stabilizing influence of the characteristic favorable average magnetic field-line curvature present in tokamak plasmas).[13,26] In expression (48), $|\chi^e_k|/|E^e_{kk}|$ is the magnitude of the tearing-parity magnetic flux that would be driven at the kth rational surface by the external perturbation in the absence of any shielding at the surface (i.e., when $\tilde{\Delta}^e_k=0$). Thus, $\Sigma_k(S_k)$ can be interpreted as the "shielding factor" at the kth surface: i.e., the factor by which the flux driven at the surface is reduced by the layer response. Obviously, expression (49) is only valid when $S_k>S_{kc}$ (i.e., when the tearing-parity mode that only reconnects magnetic flux at the kth rational surface is stable). In the high Lundquist limit, $S_k\gg S_{kc}$, the magnitude of the shielding factor becomes very much less than unity. This implies that, in a high temperature tokamak plasma, there can be strong shielding of a given rational surface from a resonant external magnetic perturbation, even when the surface in question is locked to the perturbation. This shielding is due to the Glasser effect.[13] As $S_k\rightarrow S_{kc}$, the shielding factor grows in magnitude, eventually becoming infinite at the marginal stability point, $S_k=S_{kc}$. In other words, the shielding breaks down as the tearing-parity mode that reconnects flux at the kth rational surface approaches marginal stability. In fact, when the mode is close to marginal stability, the magnitude of the shielding factor becomes greater than unity, indicating that the layer response actually amplifies the reconnected magnetic flux driven at the kth rational surface.

Suppose that the tearing-parity mode that only reconnects magnetic flux at the kth rational surface is intrinsically stable: i.e., $E^e_{kk}<0$.[21] In this situation, Eq. (46) becomes

$$\Psi^e_k \simeq -\frac{\chi^e_k}{|E^e_{kk}|}\,\Sigma_k(S_k), \tag{51}$$

where

$$\Sigma_k(S_k)=\frac{1}{(S_k/S_{kc})^{\mu_k}+1} \tag{52}$$

and

$$S_{kc}=\left(\frac{|E^e_{kk}|}{\tilde{\Delta}^e_{kc}}\right)^{1/\mu_k}. \tag{53}$$

In the high Lundquist limit, $S_k\gg S_{kc}$, the magnitude of the shielding factor, $\Sigma_k(S_k)$, is very much less than unity: i.e., there is strong shielding. On the other hand, in the low Lundquist number limit, $S_k\ll S_{kc}$, the magnitude of the shielding factor is unity: i.e., there is no shielding. Hence, we can interpret S_{kc} as the critical Lundquist number at the kth rational surface above which there is strong shielding due to the Glasser effect.

For the example equilibrium illustrated in Figs. 1 and 2, $E^e_{11}=3.685$ and $E^e_{22}=-6.424$. We also have $\mu_1=0.338$, $\tilde{\Delta}^e_{1c}=2.531\times10^{-2}$, $\tilde{\Omega}_{1c}=\pm1.606\times10^{-2}$, $\mu_2=0.335$, $\tilde{\Delta}^e_{2c}=1.287\times10^{-2}$, and $\tilde{\Omega}_{2c}=\pm6.970\times10^{-3}$. Thus, $S_{1c}=2.49\times10^6$ and $S_{2c}=1.14\times10^8$. It follows that the shielding factor at the $q=2$ surface (assuming that this surface is locked, and the plasma at the $q=3$ surface is rapidly rotating: i.e., $|\tilde{\Omega}_2|\gg|\tilde{\Omega}_{2c}|$) is

$$\Sigma_1(S_1)=\frac{1}{\left(S_1/2.49\times10^6\right)^{0.338}-1}. \tag{54}$$

(Obviously, if the $q=2$ surface is not locked then the shielding factor will be smaller: i.e., there will be more shielding.

Thus, the above expression specifies the least possible amount of shielding at the $q=2$ surface.) On the other hand, the shielding factor at the $q=3$ surface (assuming that this surface is locked, and the plasma at the $q=2$ surface is rapidly rotating: i.e., $|\tilde{\Omega}_1| \gg |\tilde{\Omega}_{1c}|$) is

$$\Sigma_2(S_2) = \frac{1}{\left(S_2/1.14\times 10^8\right)^{0.335}+1}. \tag{55}$$

C. Calculation of optimal $n=1$ wall displacements

According to Eq. (26), for a wall displacement of fixed amplitude, the magnitude of the parameter χ_k^e is maximized when $\Xi_j \propto \xi_{k,j}^e$. Hence, according to Eq. (46), for a fixed plasma response, the tearing-parity magnetic flux driven at the kth rational surface is also maximized. We conclude that the Fourier harmonics of the optimal wall displacement for driving tearing-parity magnetic reconnection at the kth rational surface can be written as

$$\Xi_j = -\delta\,\hat{\xi}_{k,j}^e, \tag{56}$$

where

$$\hat{\xi}_{k,j}^e = \frac{\xi_{k,j}^e}{||\xi_k^e||} \tag{57}$$

and

$$||\xi_k^e|| = \left(\sum_{j=1,J} |\xi_{k,j}^e|^2\right)^{1/2}. \tag{58}$$

Here, δ is the mean wall displacement (in r). Thus, the optimally displaced wall lies at

$$r = a - \mathrm{Re}\sum_{j=1,J}\delta\,\hat{\xi}_{k,j}^e\,\exp\left[\mathrm{i}\left(m_j\,\theta - n\,\phi\right)\right]. \tag{59}$$

If the $\hat{\xi}_{k,j}^e$ are real (which is the case when the plasma equilibrium is up-down symmetric), then the optimally displaced wall lies at

$$r = a + \delta\left[C_k(\theta)\,\cos(n\,\phi) + S_k(\theta)\,\sin(n\,\phi)\right]. \tag{60}$$

Here,

$$C_k(\theta) = \sum_{j=1,J}\hat{\xi}_{k,j}\,\cos\left(m_j\,\theta\right), \tag{61}$$

$$S_k(\theta) = \sum_{j=1,J}\hat{\xi}_{k,j}\,\sin\left(m_j\,\theta\right). \tag{62}$$

Finally, from (48) and (51), if the wall is optimally displaced, then the tearing-parity magnetic flux driven at the kth rational surface is

$$\Psi_k^e = \delta\,\frac{||\xi_k^e||}{|E_{kk}^e|}\,\Sigma_k(S_k). \tag{63}$$

Figures 5 and 6 show the optimal $n=1$ wall displacement for driving tearing-parity magnetic flux at the $q=2$ surface, calculated for our example equilibrium. It can be seen

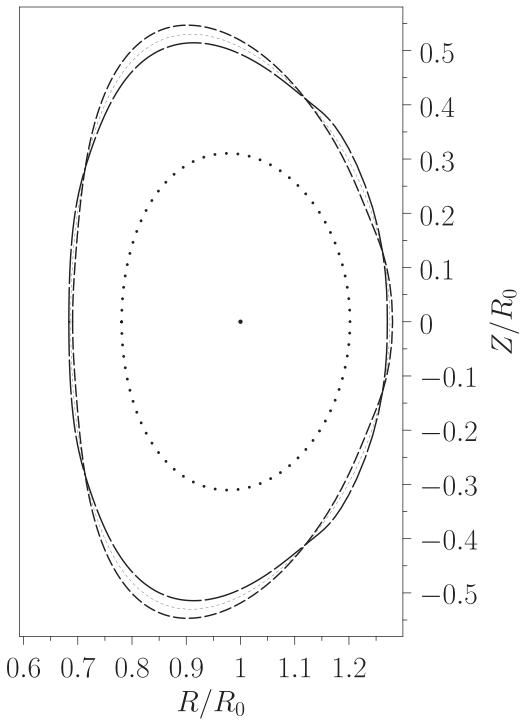

FIG. 5. The optimal $n=1$ wall displacement for driving tearing-parity magnetic flux at the $q=2$ surface calculated for a plasma equilibrium characterized by $\bar{a}=0.3$, $\kappa=1.8$, $\bar{\delta}=0.25$, $s_b=0.95$, $q_0=1.05$, $q_b=3.95$, and $\beta_N=0.25$. The thin dashed curve shows $r=a$. The thick dashed curves show $r=a\pm\delta\,C_1(\theta)$, where $\delta=0.025$. Finally, the dotted curve shows the location of the $q=2$ surface.

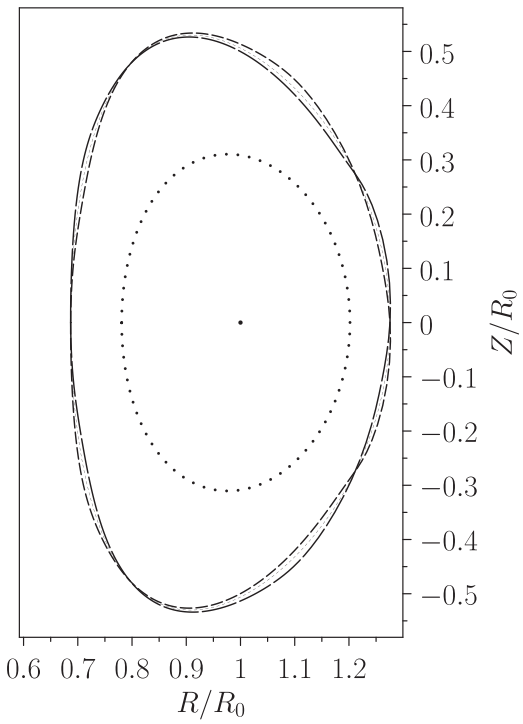

FIG. 6. The optimal $n=1$ wall displacement for driving tearing-parity magnetic flux at the $q=2$ surface calculated for a plasma equilibrium characterized by $\bar{a}=0.3$, $\kappa=1.8$, $\bar{\delta}=0.25$, $s_b=0.95$, $q_0=1.05$, $q_b=3.95$, and $\beta_N=0.25$. The thin dashed curve shows $r=a$. The thick dashed curves show $r=a\pm\delta\,S_1(\theta)$, where $\delta=0.025$. Finally, the dotted curve shows the location of the $q=2$ surface.

that the optimal displacement takes the form of a distorted $m = 3/n = 1$ helical oscillation in the geometric poloidal and toroidal angles. Figures 7 and 8 show the optimal $n = 1$ wall displacement for driving tearing-parity magnetic flux at the $q = 3$ surface, calculated for the same equilibrium. In this case, the optimal displacement takes the form of a distorted $m = 4/n = 1$ helical oscillation in the geometric poloidal and toroidal angles. Both cases are indicative of a coupling between the m/n and $m+1, n$ harmonics mediated by the $m = 1$, $n = 0$ Shafranov shift of the equilibrium. Furthermore, in both cases, the distortion is such that the amplitude of the oscillation is particularly large above and below the plasma and particularly small on the inboard side.[32] The fact that the amplitude of the oscillation is particularly large above and below the plasma could indicate that the $q = 2$ and $q = 3$ surfaces respond preferentially to $n = 1$ wall displacements above and below the plasma. Alternatively, this effect may just be an artifact of flux expansion above and below the plasma (the equilibrium magnetic flux surfaces are relatively further apart above and below the plasma, so a larger displacement is required to produce a given response at the $q = 2$ and $q = 3$ surfaces). On the other hand, there seems little doubt that the $q = 2$ and $q = 3$ surfaces respond preferentially to $n = 1$ wall displacements on the outboard, rather than the inboard, side of the plasma. This preference may be related to the previously mentioned coupling via the $m = 1, n = 0$ equilibrium harmonic, which tends to cause m, n and $m+1, n$ modes to phase-lock such that they interfere constructively on the onboard side of the plasma.[33]

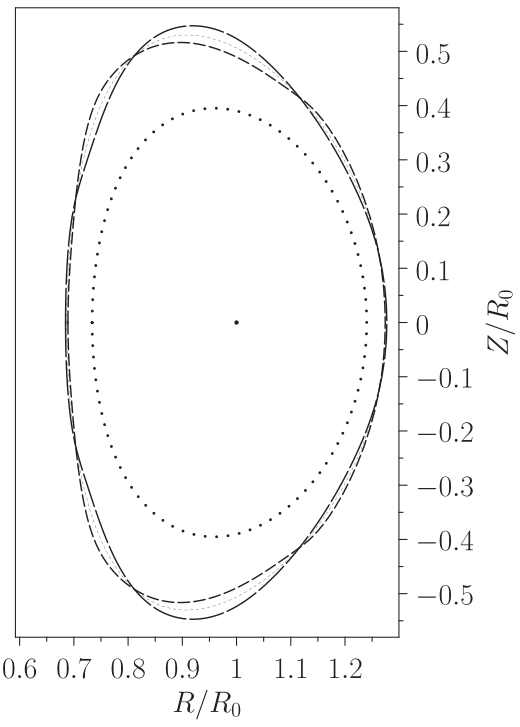

FIG. 7. The optimal $n = 1$ wall displacement for driving tearing-parity magnetic flux at the $q = 3$ surface calculated for a plasma equilibrium characterized by $\bar{a} = 0.3$, $\kappa = 1.8$, $\bar{\delta} = 0.25$, $s_b = 0.95$, $q_0 = 1.05$, $q_b = 3.95$, and $\beta_N = 0.25$. The thin dashed curve shows $r = a$. The thick dashed curves show $r = a \pm \delta\, C_2(\theta)$, where $\delta = 0.025$. Finally, the dotted curve shows the location of the $q = 3$ surface.

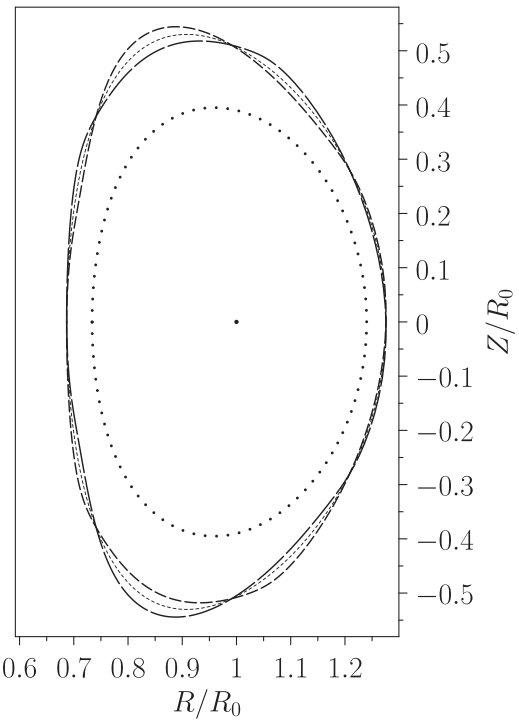

FIG. 8. The optimal $n = 1$ wall displacement for driving tearing-parity magnetic flux at the $q = 3$ surface calculated for a plasma equilibrium characterized by $\bar{a} = 0.3$, $\kappa = 1.8$, $\bar{\delta} = 0.25$, $s_b = 0.95$, $q_0 = 1.05$, $q_b = 3.95$, and $\beta_N = 0.25$. The thin dashed curve shows $r = a$. The thick dashed curves show $r = a \pm \delta\, S_2(\theta)$, where $\delta = 0.025$. Finally, the dotted curve shows the location of the $q = 3$ surface.

VII. BETA SCAN

Consider a series of plasma equilibria, characterized by $\bar{a} = 0.3$, $\kappa = 1.8$, $s_b = 0.95$, $\bar{\delta} = 0.25$, $q_0 = 1.05$, and $q_b = 3.95$, for which the normal beta, β_N, varies between zero and the $n = 1$ ideal beta-limit, $\beta_{Nc} = 2.955$. The example equilibrium considered in Sec. VI is a member of this series corresponding to $\beta_N = 0.25$.

Figure 9 shows the shielding factor for tearing-parity magnetic flux driven at the $q = 2$ surface by an $n = 1$ wall displacement, calculated for the series of equilibria in question. Figure 10 shows the corresponding ratio of the flux driven at the $q = 2$ surface to the mean wall displacement, when the wall displacement is optimal. It can be seen that strong shielding (i.e., $\Sigma_1 \ll 1$) is achieved at intermediate β_N values when the local Lundquist number is relatively high (i.e., $S_1 \gg 10^6$), but that the shielding is always weak (i.e., $\Sigma_1 \sim 1$) when the local Lundquist number is relatively low (i.e., $S_1 \sim 10^6$). Furthermore, the shielding breaks down completely and actually becomes amplification (i.e., $\Sigma_1 \gg 1$), both in the low-β limit, $\beta_N \to 0$, and in the high-β limit, $\beta_N \to \beta_{Nc}$. The shielding breaks down in the low-β limit because the Glasser effect (which depends on the local pressure gradient) becomes too feeble to stabilize the $n = 1$ tearing mode that only reconnects flux at the $q = 2$ surface (which is intrinsically unstable: i.e., $E^e_{11} > 0$). The shielding breaks down in the high-β limit because the tearing stability index E^e_{11} tends to infinity as $\beta_N \to \beta_{Nc}$.[34] Figures 9 and 10 suggest that the well-known susceptibility of low-β startup plasmas to highly amplified locked modes[3–8] may be due to the breakdown of Glasser-effect shielding of an intrinsically

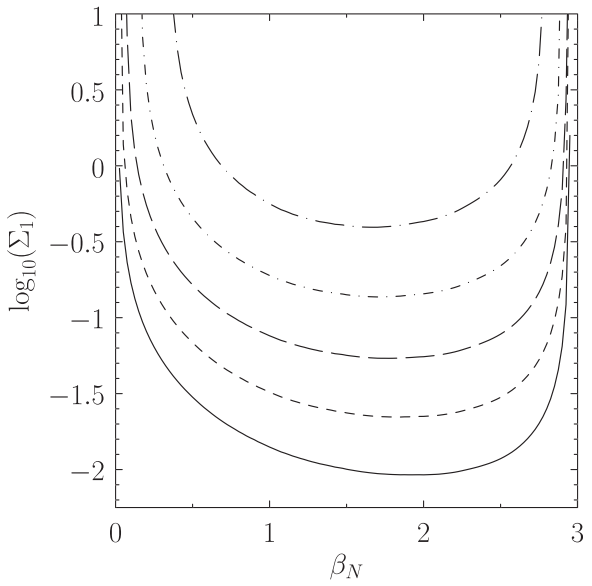

FIG. 9. The shielding factor for tearing-parity magnetic flux driven at the $q=2$ surface by an $n=1$ wall displacement calculated as a function of the normal beta for a series of plasma equilibria characterized by $\bar{a}=0.3$, $\kappa=1.8$, $\bar{\delta}=0.25$, $s_b=0.95$, $q_0=1.05$, and $q_b=3.95$. The solid, short-dashed, long-dashed, dot-short-dashed, and dot-long-dashed curves correspond to $S_1=10^{10}$, 10^9, 10^8, 10^7, and 10^6, respectively.

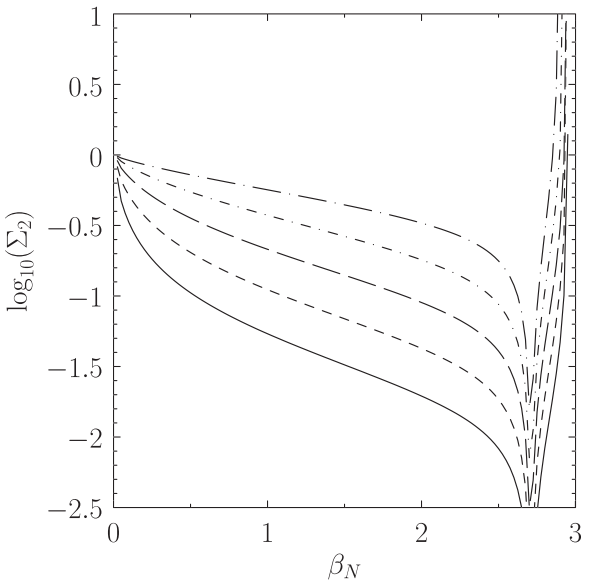

FIG. 11. The shielding factor for tearing-parity magnetic flux driven at the $q=3$ surface by an $n=1$ wall displacement calculated as a function of the normal beta for a series of plasma equilibria characterized by $\bar{a}=0.3$, $\kappa=1.8$, $\bar{\delta}=0.25$, $s_b=0.95$, $q_0=1.05$, and $q_b=3.95$. The solid, short-dashed, long-dashed, dot-short-dashed, and dot-long-dashed curves correspond to $S_1=10^{10}$, 10^9, 10^8, 10^7, and 10^6, respectively.

unstable tearing mode from a resonant error-field, as the plasma pressure becomes too low. The figures also account for the common appearance of highly amplified locked modes in tokamak plasmas that approach the ideal β-limit.[9–11]

Figure 11 shows the shielding factor for tearing-parity magnetic flux driven at the $q=3$ surface by an $n=1$ wall displacement, calculated for the series of equilibria in question. Figure 12 shows the corresponding ratio of the flux driven at the $q=3$ surface to the mean wall displacement, when the wall displacement is optimal. It can be seen that, although the shielding fails (i.e., $\Sigma_2\rightarrow 1$) as $\beta_N\rightarrow 0$, there is no amplification of the driven magnetic flux in this limit, because the $n=1$ tearing mode that only reconnects magnetic flux at the $q=3$ surface is intrinsically stable (i.e., $E^e_{22}<0$) at low-β. On the other hand, there is again strong amplification of the flux driven at the $q=3$ surface when the plasma approaches the ideal β-limit.

Figures 13 and 14 show the optimal $n=1$ wall displacement for driving tearing-parity magnetic flux at the $q=2$

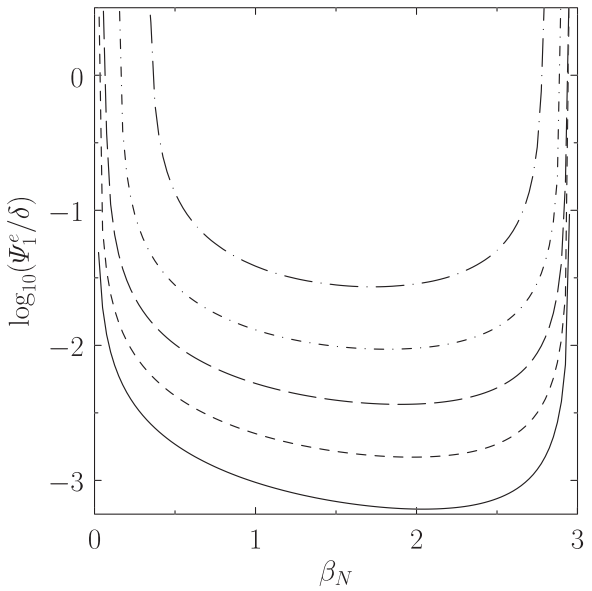

FIG. 10. The ratio of the tearing-parity magnetic flux driven at the $q=2$ surface by an optimal $n=1$ wall displacement to the mean wall displacement calculated as a function of the normal beta for a series of plasma equilibria characterized by $\bar{a}=0.3$, $\kappa=1.8$, $\bar{\delta}=0.25$, $s_b=0.95$, $q_0=1.05$, and $q_b=3.95$. The solid, short-dashed, long-dashed, dot-short-dashed, and dot-long-dashed curves correspond to $S_1=10^{10}$, 10^9, 10^8, 10^7, and 10^6, respectively.

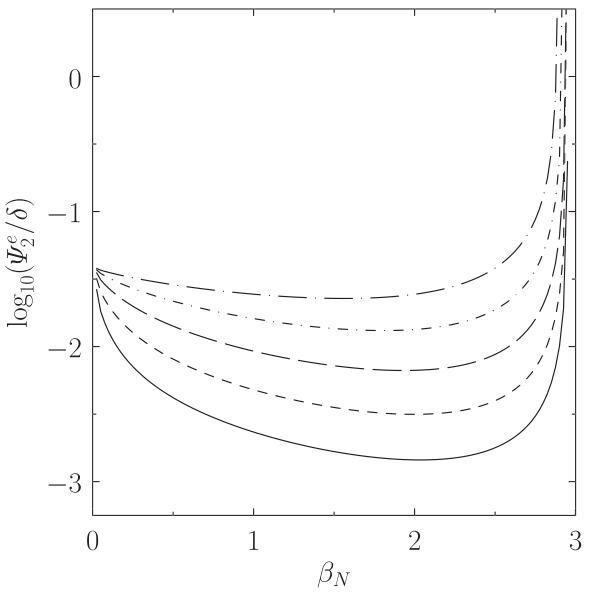

FIG. 12. The ratio of the tearing-parity magnetic flux driven at the $q=3$ surface by an optimal $n=1$ wall displacement to the mean wall displacement calculated as a function of the normal beta for a series of plasma equilibria characterized by $\bar{a}=0.3$, $\kappa=1.8$, $\bar{\delta}=0.25$, $s_b=0.95$, $q_0=1.05$, and $q_b=3.95$. The solid, short-dashed, long-dashed, dot-short-dashed, and dot-long-dashed curves correspond to $S_1=10^{10}$, 10^9, 10^8, 10^7, and 10^6, respectively.

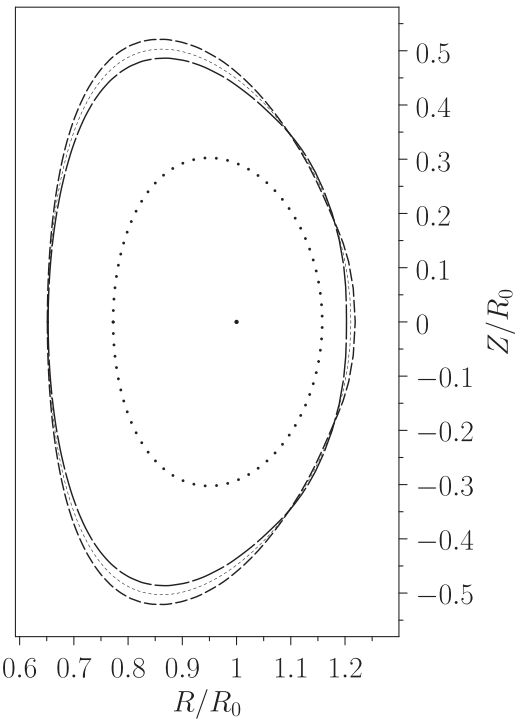

FIG. 13. The optimal $n=1$ wall displacement for driving tearing-parity magnetic flux at the $q=2$ surface calculated for a plasma equilibrium characterized by $\bar{a}=0.3$, $\kappa=1.8$, $\bar{\delta}=0.25$, $s_b=0.95$, $q_0=1.05$, $q_b=3.95$, and $\beta_N=3.95$. The thin dashed curve shows $r=a$. The thick dashed curves show $r=a\pm\delta\,C_1(\theta)$, where $\delta=0.025$. Finally, the dotted curve shows the location of the $q=2$ surface.

surface, calculated when the plasma lies very close to the ideal β-limit. Likewise, Figs. 15 and 16 show the optimal $n=1$ wall displacement for driving tearing-parity magnetic flux at the $q=3$ surface. In both cases, the optimal displacement takes the form of a distorted $m=3/n=1$ helical oscillation in the geometric poloidal and toroidal angles. The distortion is such that the amplitude of the oscillation is particularly large above and below the plasma, and on the outboard side, but is virtually zero on the inboard side.[32] This indicates that, close to the β-limit, the $q=2$ and $q=3$ surfaces respond preferentially to $n=1$ wall displacements above and below the plasma (however, see the caveat at the end of Sec. VI C), and on the outboard side, but are completely insensitive to wall displacements on the inboard side.[32]

Note that Figs. 13 and 15 are virtually identical to one another. The same can be said for Figs. 14 and 16. This suggests that, when the plasma is close to the ideal β-limit, the optimal $n=1$ wall displacement for driving tearing-parity magnetic flux at the $q=2$ surface is very similar in shape to the optimal displacement for driving flux at the $q=3$ surface. In fact, we can measure this similarity by defining the correlation factor

$$\alpha_{12}=\left|\sum_{j=1,J}\hat{\xi}_{1j}\,\hat{\xi}_{2j}\right|. \tag{64}$$

Thus, if $\alpha_{12}=0$ then there is no similarity between the two shapes, whereas if $\alpha_{12}=1$ then the two shapes are identical. The correlation factor, calculated for the series of plasma equilibria in question, is shown in Fig. 17. It can be seen that at low-β the correlation factor is relatively small (i.e.,

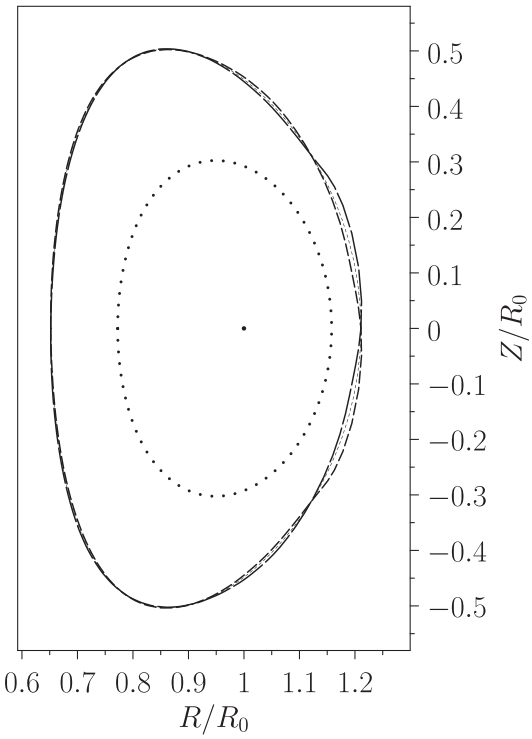

FIG. 14. The optimal $n=1$ wall displacement for driving tearing-parity magnetic flux at the $q=2$ surface calculated for a plasma equilibrium characterized by $\bar{a}=0.3$, $\kappa=1.8$, $\bar{\delta}=0.25$, $s_b=0.95$, $q_0=1.05$, $q_b=3.95$, and $\beta_N=3.95$. The thin dashed curve shows $r=a$. The thick dashed curves show $r=a\pm\delta\,S_1(\theta)$, where $\delta=0.025$. Finally, the dotted curve shows the location of the $q=2$ surface.

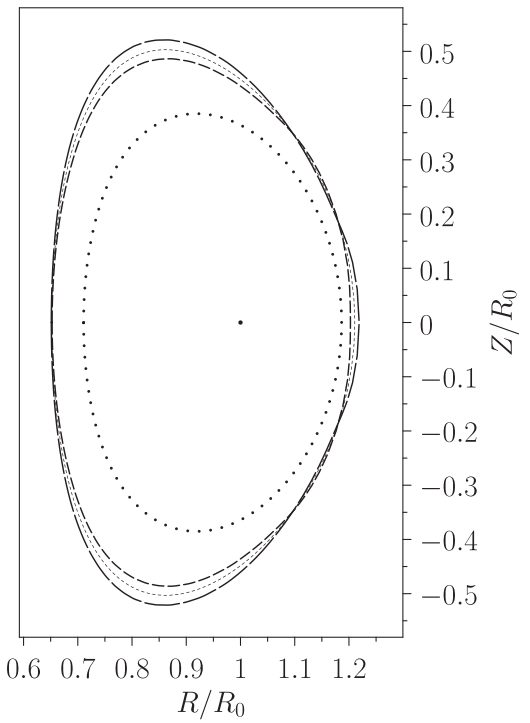

FIG. 15. The optimal $n=1$ wall displacement for driving tearing-parity magnetic flux at the $q=3$ surface calculated for a plasma equilibrium characterized by $\bar{a}=0.3$, $\kappa=1.8$, $\bar{\delta}=0.25$, $s_b=0.95$, $q_0=1.05$, $q_b=3.95$, and $\beta_N=3.95$. The thin dashed curve shows $r=a$. The thick dashed curves show $r=a\pm\delta\,C_2(\theta)$, where $\delta=0.025$. Finally, the dotted curve shows the location of the $q=3$ surface.

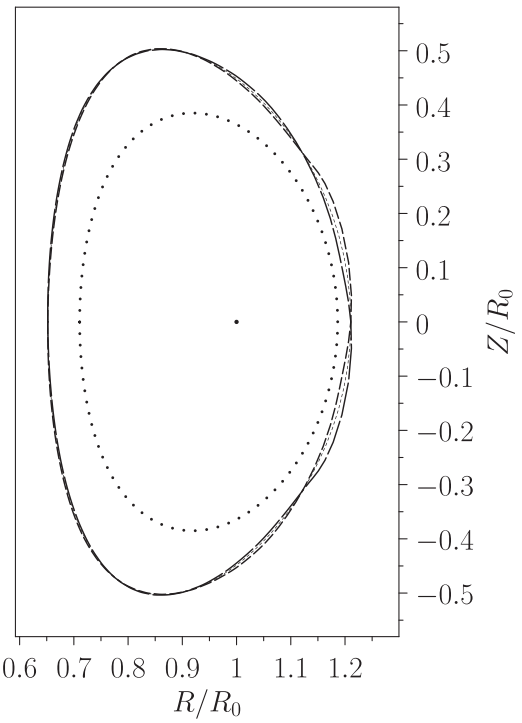

FIG. 16. The optimal $n=1$ wall displacement for driving tearing-parity magnetic flux at the $q=3$ surface calculated for a plasma equilibrium characterized by $\bar{a}=0.3$, $\kappa=1.8$, $\bar{\delta}=0.25$, $s_b=0.95$, $q_0=1.05$, $q_b=3.95$, and $\beta_N=3.95$. The thin dashed curve shows $r=a$. The thick dashed curves show $r=a\pm\delta S_2(\theta)$, where $\delta=0.025$. Finally, the dotted curve shows the location of the $q=3$ surface.

$0<\alpha_{12}\ll 1$), indicating that in this limit the optimal $n=1$ wall displacement for driving flux at the $q=2$ surface has a quite different shape to that for driving flux at the $q=3$ surface. On the other hand, the correlation factor approaches unity as the ideal β-limit is approached, indicating that in this limit the optimal $n=1$ wall displacement shape for driving flux at the $q=2$ surface becomes identical to that for driving flux at the $q=3$ surface. One possible explanation for this behavior is that, close to the β-limit, both surfaces are responding preferentially to a displacement that couples strongly to the marginally stable ideal eigenfunction.[18]

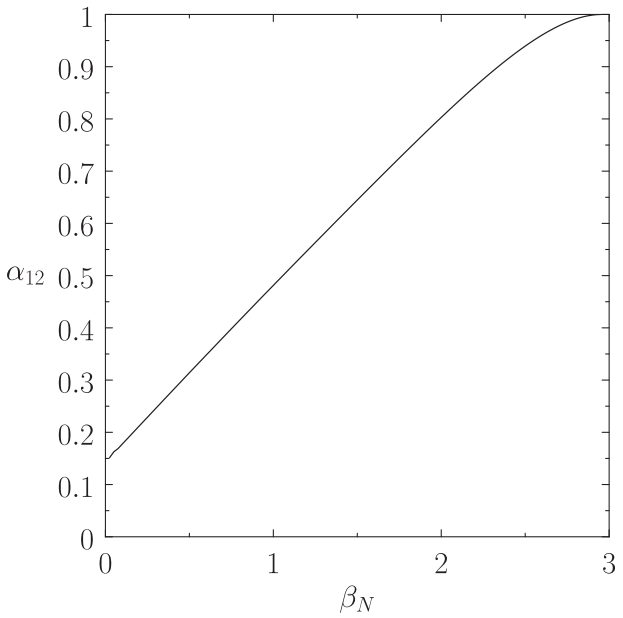

FIG. 17. The correlation factor between the optimal $n=1$ wall displacement shapes required to drive tearing-parity magnetic flux at the $q=2$ and the $q=3$ surfaces calculated as a function of the normal beta for a series of plasma equilibria characterized by $\bar{a}=0.3$, $\kappa=1.8$, $\bar{\delta}=0.25$, $s_b=0.95$, $q_0=1.05$, and $q_b=3.95$.

VIII. SUMMARY AND DISCUSSION

This paper discusses the use of asymptotic matching techniques to determine the response of a high temperature tokamak plasma with a realistic equilibrium to an externally generated, non-axisymmetric, static, magnetic perturbation. The plasma is divided into two regions. In the outer region, which comprises most of the plasma, the response is governed by the linearized, marginally stable, ideal-MHD equations. In the inner region, which is strongly localized around the various rational surfaces within the plasma (where the marginally stable, ideal-MHD equations become singular), the response is obtained from Glasser-Greene-Johnson linear layer physics.[26] For the sake of simplicity, we have focused on the situation where the plasma at one of the internal rational surfaces is locked to the external perturbation, whereas that at the other surfaces is rotating.

In agreement with Liu *et al.*,[13] we find that, under certain circumstances, the so-called Glasser effect[26] leads to strong shielding of the plasma in the vicinity of an internal rational surface from an externally generated, non-axisymmetric, static, magnetic perturbation. This is true even in the limit in which the plasma at the rational surface is locked to the perturbation. Such shielding breaks down at low-β, because the Glasser effect becomes too weak. The shielding also breaks down as the ideal β-limit is approached, because the plasma becomes too unstable.

By supposing that the static external magnetic perturbation is generated by a small amplitude, non-axisymmetric, displacement in a perfectly conducting wall surrounding (but, not, necessarily touching) the plasma, it is possible to determine the optimal $n=1$ wall displacement for driving magnetic reconnection at a given rational surface within the plasma. At low-β, the optimum displacements for driving magnetic reconnection at different rational surfaces are quite distinct from one another. On the other hand, as the ideal β-limit is approached, the optimum displacements all become identical.

The calculations discussed in this paper could be extended in a number of different ways. For instance, we could use the Glasser-Greene-Johnson linear layer model to investigate the efficacy of plasma rotation as a mechanism for shielding the internal rational surfaces of a plasma from an externally generated, non-axisymmetric, static, magnetic perturbation. Alternatively, we could replace the Glasser-Greene-Johnson layer model by its nonlinear generalization.[35,36] This would enable us to determine the efficacy of both magnetic curvature and plasma rotation as shielding mechanisms in the nonlinear limit in which the locked island widths at the various internal rational surfaces exceed the linear layer widths. Finally, we could dispense with the perfectly conducting wall, and, instead, consider a plasma surrounded by a vacuum region that extends to infinity.

ACKNOWLEDGMENTS

This research was funded by the U.S. Department of Energy under Contract No. DE-FG02-04ER-54742.

APPENDIX A: SOLUTION OF LINEARIZED MARGINALLY STABLE IDEAL-MHD EQUATIONS

1. Normalization and coordinates

All lengths are normalized to the major radius of the plasma magnetic axis, R_0, all magnetic field-strengths to the vacuum toroidal field-strength at the magnetic axis, B_0, and all plasma pressures to B_0^2/μ_0.

Let R, ϕ, Z be right-handed cylindrical coordinates whose symmetry axis corresponds to the toroidal symmetry axis of the plasma. The Jacobian for these coordinates is

$$(\nabla R\times\nabla\phi\cdot\nabla Z)^{-1}=R. \tag{A1}$$

Let r, θ, ϕ be right-handed flux coordinates whose Jacobian is[19,21]

$$\mathcal{J}(r,\theta)\equiv(\nabla r\times\nabla\theta\cdot\nabla\phi)^{-1}=r\,R^2. \tag{A2}$$

Here, r is a flux-surface label with dimensions of length. Furthermore, θ is a straight poloidal angle. Let $r=0$ correspond to the magnetic axis and $\theta=0$ to the inboard midplane.

2. Plasma equilibrium

Consider an axisymmetric tokamak plasma equilibrium. The magnetic field is written as[19,21]

$$\mathbf{B}(r,\theta)=f(r)\,\nabla\phi\times\nabla r+g(r)\,\nabla\phi=f\,\nabla(\phi-q\,\theta)\times\nabla r, \tag{A3}$$

where

$$q(r)=\frac{r\,g}{f} \tag{A4}$$

is the safety-factor profile.

Equilibrium force balance yields the Grad-Shafranov equation,[19,21]

$$\frac{1}{r}\frac{\partial}{\partial r}\left(r f\,|\nabla r|^2\right)+\frac{1}{r}\frac{\partial}{\partial\theta}\left(r f\,\nabla r\cdot\nabla\theta\right)+\frac{g\,g'}{f}+R^2\,\frac{P'}{f}=0, \tag{A5}$$

where $P(r)$ is the plasma pressure profile, and $'\equiv d/dr$.

3. Governing equations

Consider a small-amplitude, non-axisymmetric, perturbation to the previously described plasma equilibrium. The system is conveniently divided into an outer region and an inner region.[25] The outer region comprises all of the plasma, and any surrounding vacuum, except a number of radially thin layers centered on the various rational surfaces (see Appendix A 5). The inner region consists of the aforementioned layers. The perturbation in the outer region is governed by linearized, marginally stable, ideal-MHD, whereas that in the inner region is governed by either linear or nonlinear resistive-MHD.[25] The overall solution is constructed by asymptotically matching the ideal-MHD solution in the outer region to the resistive-MHD solutions in the various segments of the inner region.

The linearized, marginally stable, ideal-MHD equations that govern the perturbation in the outer region are[25]

$$\delta\mathbf{B}=\nabla\times(\boldsymbol{\xi}\times\mathbf{B}), \tag{A6}$$

$$\nabla\delta P=\delta\mathbf{J}\times\mathbf{B}+\mathbf{J}\times\delta\mathbf{B}, \tag{A7}$$

$$\delta\mathbf{J}=\nabla\times\delta\mathbf{B}, \tag{A8}$$

$$\delta P=-\boldsymbol{\xi}\cdot\nabla P. \tag{A9}$$

Here, $\mathbf{J}=\nabla\times\mathbf{B}$ is the equilibrium current density. Moreover, $\boldsymbol{\xi}$, $\delta\mathbf{B}$, $\delta\mathbf{J}$, and δP are the plasma displacement, perturbed magnetic field, perturbed current density, and perturbed pressure, respectively.

4. Fourier transformed equations

Let

$$f\,\boldsymbol{\xi}\cdot\nabla r=y(r,\theta)\,\exp(-\mathrm{i}\,n\,\phi), \tag{A10}$$

$$R^2\,\delta\mathbf{B}\cdot\nabla\phi=z(r,\theta)\,\exp(-\mathrm{i}\,n\,\phi), \tag{A11}$$

where $n>0$ is the toroidal mode number of the non-axisymmetric perturbation. After considerable algebra, Eqs. (A6)–(A9) reduce to[19,21]

$$r\frac{\partial}{\partial r}\left[\left(\frac{\partial}{\partial\theta}-\mathrm{i}\,n\,q\right)y\right]=\frac{\partial}{\partial\theta}\left(Q\frac{\partial z}{\partial\theta}\right)+S\,z-\frac{\partial}{\partial\theta}\times\left[T\left(\frac{\partial}{\partial\theta}-\mathrm{i}\,n\,q\right)y+U\,y\right], \tag{A12}$$

$$\left(\frac{\partial}{\partial\theta}-\mathrm{i}\,n\,q\right)r\,\frac{\partial z}{\partial r}=-\left(\frac{\partial}{\partial\theta}-\mathrm{i}\,n\,q\right)T^*\,\frac{\partial z}{\partial\theta}+U\,\frac{\partial z}{\partial\theta}+X\,y-\left(\frac{\partial}{\partial\theta}-\mathrm{i}\,n\,q\right)V\left(\frac{\partial}{\partial\theta}-\mathrm{i}\,n\,q\right)y+W\left(\frac{\partial}{\partial\theta}-\mathrm{i}\,n\,q\right)y, \tag{A13}$$

where

$$Q(r,\theta)=\frac{1}{\mathrm{i}\,n\,|\nabla r|^2}, \tag{A14}$$

$$S(r,\theta)=\mathrm{i}\,n\,\alpha_\epsilon, \tag{A15}$$

$$T(r,\theta)=\frac{r\,\nabla r\cdot\nabla\theta}{|\nabla r|^2}-\frac{\alpha_g}{\mathrm{i}\,n\,|\nabla r|^2}, \tag{A16}$$

$$U(r,\theta)=\frac{\alpha_p\,R^2}{|\nabla r|^2}, \tag{A17}$$

$$V(r,\theta)=\frac{1}{|\nabla r|^2}\left(\frac{\mathrm{i}\,n}{R^2}+\frac{\alpha_g^2}{\mathrm{i}\,n}\right), \tag{A18}$$

$$W(r,\theta)=\frac{2\,\alpha_g\,\alpha_p\,R^2}{|\nabla r|^2}-r\,\frac{d\alpha_g}{dr}, \tag{A19}$$

$$X(r,\theta) = \mathrm{i}\, n\, \alpha_p \left[\frac{\partial}{\partial\theta}(T^* R^2) + r\frac{\partial R^2}{\partial r} - \alpha_f R^2 - U R^2\right], \quad \text{(A20)}$$

and

$$\alpha_\epsilon(r) = r^2, \quad \text{(A21)}$$

$$\alpha_g(r) = \frac{1}{f}\frac{dg}{dr}, \quad \text{(A22)}$$

$$\alpha_p(r) = \frac{r}{f^2}\frac{dP}{dr}, \quad \text{(A23)}$$

$$\alpha_f(r) = \frac{r^2}{f}\frac{d}{dr}\left(\frac{f}{r}\right). \quad \text{(A24)}$$

Let

$$y(r,\theta) = \sum_{j=1,J} y_j(r)\exp\bigl(\mathrm{i}\, m_j\,\theta\bigr), \quad \text{(A25)}$$

$$z(r,\theta) = \sum_{j=1,J} z_j(r)\exp\bigl(\mathrm{i}\, m_j\,\theta\bigr), \quad \text{(A26)}$$

where the m_j, for $j = 1, J$, are the various coupled poloidal harmonics included in the calculation. Equations (A12) and (A13) reduce to

$$r\frac{d}{dr}\left[(m_j - n\,q)\, y_j\right] = \sum_{j'=1,J}(B_{jj'}\, z_{j'} + C_{jj'}\, y_{j'}), \quad \text{(A27)}$$

$$(m_j - n\,q)\, r\frac{dz_j}{dr} = \sum_{j'=1,J}(D_{jj'}\, z_{j'} + E_{jj'}\, y_{j'}), \quad \text{(A28)}$$

for $j = 1, J$, where

$$B_{jj'}(r) = \frac{1}{2\pi\,\mathrm{i}}\oint \mathrm{e}^{-\mathrm{i}m_j\theta}\left(\frac{\partial}{\partial\theta}\, Q\, \frac{\partial}{\partial\theta} + S\right)\mathrm{e}^{\mathrm{i}m_{j'}\theta}\, d\theta, \quad \text{(A29)}$$

$$C_{jj'}(r) = \frac{1}{2\pi\,\mathrm{i}}\oint \mathrm{e}^{-\mathrm{i}m_j\theta}\left[-\frac{\partial}{\partial\theta}\, T\left(\frac{\partial}{\partial\theta} - \mathrm{i}\, n\, q\right) - \frac{\partial U}{\partial\theta}\right]\mathrm{e}^{\mathrm{i}m_{j'}\theta}\, d\theta, \quad \text{(A30)}$$

$$D_{jj'}(r) = \frac{1}{2\pi\,\mathrm{i}}\oint \mathrm{e}^{-\mathrm{i}m_j\theta}\left[-\left(\frac{\partial}{\partial\theta} - \mathrm{i}\, n\, q\right)T^*\, \frac{\partial}{\partial\theta} + U\, \frac{\partial}{\partial\theta}\right]\mathrm{e}^{\mathrm{i}m_{j'}\theta}\, d\theta, \quad \text{(A31)}$$

$$E_{jj'}(r) = \frac{1}{2\pi\,\mathrm{i}}\oint \mathrm{e}^{-\mathrm{i}m_j\theta}\left[-\left(\frac{\partial}{\partial\theta} - \mathrm{i}\, n\, q\right)V\left(\frac{\partial}{\partial\theta} - \mathrm{i}\, n\, q\right) + W\left(\frac{\partial}{\partial\theta} - \mathrm{i}\, n\, q\right) + X\right]\mathrm{e}^{\mathrm{i}m_{j'}\theta}\, d\theta. \quad \text{(A32)}$$

Hence, it follows from Eqs. (A14)–(A20) that

$$n\, B_{jj'} = m_j\, m_{j'}\, c_{jj'} + n^2\, \alpha_\epsilon\, \delta_{jj'}, \quad \text{(A33)}$$

$$C_{jj'} = m_j\,(m_{j'} - n\,q)\bigl(-f_{jj'} + n^{-1}\,\alpha_g\, c_{jj'}\bigr) - m_j\,\alpha_p\, d_{jj'}, \quad \text{(A34)}$$

$$D_{jj'} = -(m_j - n\,q)\, m_{j'}\bigl(f_{jj'} + n^{-1}\,\alpha_g\, c_{jj'}\bigr) + m_{j'}\,\alpha_p\, d_{jj'}, \quad \text{(A35)}$$

$$n^{-1}\, E_{jj'} = (m_j - n\,q)\,(m_{j'} - n\,q)\Bigl(b_{jj'} - n^{-2}\,\alpha_g^2\, c_{jj'}\Bigr) - (m_{j'} - n\,q)\, n^{-1}\, r\,\frac{d\alpha_g}{dr}\,\delta_{jj'} + \alpha_p[(m_j - m_{j'})\, g_{jj'} + n^{-1}\,\alpha_g\,(m_j + m_{j'} - 2\,n\,q)\, d_{jj'} + r\,\frac{da_{jj'}}{dr} - \alpha_f\, a_{jj'} - \alpha_p\, e_{jj'}\bigr], \quad \text{(A36)}$$

where

$$a_{jj'}(r) = \oint R^2\exp\bigl[-\mathrm{i}\,(m_j - m_{j'})\,\theta\bigr]\frac{d\theta}{2\pi}, \quad \text{(A37)}$$

$$b_{jj'}(r) = \oint |\nabla r|^{-2}\, R^{-2}\exp\bigl[-\mathrm{i}\,(m_j - m_{j'})\,\theta\bigr]\frac{d\theta}{2\pi}, \quad \text{(A38)}$$

$$c_{jj'}(r) = \oint |\nabla r|^{-2}\exp[-\mathrm{i}\,(m - m')\,\theta]\frac{d\theta}{2\pi}, \quad \text{(A39)}$$

$$d_{jj'}(r) = \oint |\nabla r|^{-2}\, R^2\exp\bigl[-\mathrm{i}\,(m_j - m_{j'})\,\theta\bigr]\frac{d\theta}{2\pi}, \quad \text{(A40)}$$

$$e_{jj'}(r) = \oint |\nabla r|^{-2}\, R^4\exp\bigl[-\mathrm{i}\,(m_j - m_{j'})\,\theta\bigr]\frac{d\theta}{2\pi}, \quad \text{(A41)}$$

$$f_{jj'}(r) = \oint \frac{\mathrm{i}\, r\,\nabla r\cdot\nabla\theta}{|\nabla r|^2}\exp\bigl[-\mathrm{i}\,(m_j - m_{j'})\,\theta\bigr]\frac{d\theta}{2\pi}, \quad \text{(A42)}$$

$$g_{jj'}(r) = \oint \frac{\mathrm{i}\, r\,\nabla r\cdot\nabla\theta}{|\nabla r|^2}\, R^2\exp\bigl[-\mathrm{i}\,(m_j - m_{j'})\,\theta\bigr]\frac{d\theta}{2\pi}. \quad \text{(A43)}$$

Let

$$y_j = \frac{\psi_j(r)}{m_j - n\,q}, \quad \text{(A44)}$$

$$z_j = n\,\frac{Z_j(r)}{m_j - n\,q} - \frac{C_{jj}}{B_{jj}}\,\frac{\psi_j(r)}{m_j - n\,q}. \quad \text{(A45)}$$

It follows that

$$\delta\mathbf{B}\cdot\nabla r = \mathrm{i}\, R^{-2}\sum_{j=1,J}\frac{\psi_j}{r}\exp\bigl[\mathrm{i}\,(m_j\,\theta - n\,\phi)\bigr]. \quad \text{(A46)}$$

Furthermore, Eqs. (A27) and (A28) transform to

$$r\,\frac{d\psi_j}{dr} = \sum_{j'=1,J}\frac{L_{jj'}\, Z_{j'} + M_{jj'}\,\psi_{j'}}{m_{j'} - n\,q}, \quad \text{(A47)}$$

$$(m_j - n\,q)\, r\,\frac{d}{dr}\left(\frac{Z_j}{m_j - n\,q}\right) = \sum_{j'=1,J}\frac{N_{jj'}\, Z_{j'} + P_{jj'}\,\psi_{j'}}{m_{j'} - n\,q}, \quad \text{(A48)}$$

for $j = 1, J$, where

$$L_{jj'}(r) = n\, B_{jj'}, \quad \text{(A49)}$$

$$M_{jj'}(r) = C_{jj'} + \lambda_{j'}\, L_{jj'}, \quad \text{(A50)}$$

$$N_{jj'}(r) = D_{jj'} - \lambda_j\, L_{jj'}, \quad \text{(A51)}$$

$$P_{jj'}(r) = n^{-1}\, E_{jj'} - \lambda_j\, M_{jj'} + \lambda_{j'}\, N_{jj'} + \lambda_j\,\lambda_{j'}\, L_{jj'} - \lambda_j\, n\, q\, s\,\delta_{jj'} - (m_j - n\,q)\, r\,\frac{d\lambda_j}{dr}\,\delta_{jj'}, \quad \text{(A52)}$$

with

$$s(r) = \frac{r\,q'}{q}, \tag{A53}$$

and

$$\lambda_j(r) = -\frac{C_{jj}}{n\,B_{jj}} = -\left[\frac{m_j\,(m_j - n\,q)\,n^{-1}\,\alpha_g\,c_{jj} - m\,\alpha_p\,d_{jj}}{m_j^2\,c_{jj} + n^2\,\alpha_\epsilon}\right]. \tag{A54}$$

Now, for a general plasma equilibrium, it is easily demonstrated that $a_{j'j} = a^*_{jj'}$, $b_{j'j} = b^*_{jj'}$, $c_{j'j} = c^*_{jj'}$, $d_{j'j} = d^*_{jj'}$, $e_{j'j} = e^*_{jj'}$, $f_{j'j} = -f^*_{jj'}$, $g_{j'j} = -g^*_{jj'}$, for all j, j', so that $B_{j'j} = B^*_{jj'}$, $C_{j'j} = -D^*_{jj'}$, $D_{j'j} = -C^*_{jj'}$, $E_{j'j} = E^*_{jj'}$, and

$$L_{j'j} = L^*_{jj'}, \tag{A55}$$

$$M_{j'j} = -N^*_{jj'}, \tag{A56}$$

$$N_{j'j} = -M^*_{jj'}, \tag{A57}$$

$$P_{j'j} = P^*_{jj'}. \tag{A58}$$

It follows from Eqs. (A47) and (A48) that

$$r\,\frac{d}{dr}\left(\sum_{j=1,J}\frac{Z_j^*\,\psi_j - \psi_j^*\,Z_j}{m_j - n\,q}\right) = 0. \tag{A59}$$

The net toroidal electromagnetic torque acting on the region lying within that equilibrium magnetic flux-surface whose label is r takes the form[21]

$$T_\phi(r) = \int_0^r \oint\oint R^2\,\nabla\phi\cdot(\delta\mathbf{J}\times\delta\mathbf{B})\,\mathcal{J}\,dr\,d\theta\,d\phi, \tag{A60}$$

which can be shown to reduce to

$$T_\phi(r) = n\,\pi^2\,\mathrm{i}\sum_{j=1,J}\frac{Z_j^*\,\psi_j - \psi_j^*\,Z_j}{m_j - n\,q}. \tag{A61}$$

Hence, we deduce that

$$\frac{dT_\phi}{dr} = 0 \tag{A62}$$

in the outer region.

5. Behavior in the vicinity of rational surface

Let there be K rational surfaces in the plasma. Suppose that the kth surface has the flux-surface label r_k and the resonant poloidal mode number m_k, where $q(r_k) = m_k/n$, for $k = 1, K$.

Consider the solution of the outer equations, (A47) and (A48), in the vicinity of the kth surface. Let $x = r - r_k$. The most general small-$|x|$ solution of the outer equations can be shown to take the form[21]

$$\psi_j(x) = A^{\pm}_{Lk}\,|x|^{\nu_{Lk}}\,(1 + \lambda_{Lk}\,x + \cdots) + A^{\pm}_{Sk}\,\mathrm{sgn}(x)\,|x|^{\nu_{Sk}}\,(1 + \cdots) + A_{Ck}\,x\,(1 + \cdots), \tag{A63}$$

$$Z_j(x) = A^{\pm}_{Lk}\,|x|^{\nu_{Lk}}\,(b_{Lk} + \gamma_{Lk}\,x + \cdots) + A^{\pm}_{Sk}\,\mathrm{sgn}(x)\,|x|^{\nu_{Sk}}\,(b_{Sk} + \cdots) + B_{Ck}\,x\,(1 + \cdots) \tag{A64}$$

if $m_j = m_k$, and

$$\psi_j(x) = A^{\pm}_{Lk}\,|x|^{\nu_{Lk}}\,(a_{kj} + \cdots) + \bar{\psi}_{kj}\,(1 + \cdots), \tag{A65}$$

$$Z_j(x) = A^{\pm}_{Lk}\,|x|^{\nu_{Lk}}\,(b_{kj} + \cdots) + \bar{Z}_{kj}\,(1 + \cdots) \tag{A66}$$

if $m_j \neq m_k$. Moreover, the superscripts $^+$ and $^-$ correspond to $x > 0$ and $x < 0$, respectively. Here,

$$\nu_{Lk} = \frac{1}{2} - \sqrt{-D_{Ik}}, \tag{A67}$$

$$\nu_{Sk} = \frac{1}{2} + \sqrt{-D_{Ik}}, \tag{A68}$$

$$D_{Ik} = -L_{0k}\,P_{0k} - \frac{1}{4}, \tag{A69}$$

$$L_{0k} = -\left(\frac{L_{kk}}{m_k\,s}\right)_{r_k}, \tag{A70}$$

$$P_{0k} = -\left(\frac{P_{kk}}{m_k\,s}\right)_{r_k}. \tag{A71}$$

Furthermore,

$$b_{Lk} = \frac{\nu_{Lk}}{L_{0k}}, \tag{A72}$$

$$b_{Sk} = \frac{\nu_{Sk}}{L_{0k}}, \tag{A73}$$

$$A_{Ck} = -\frac{1}{r_k\,P_{0k}}\sum_{j=1,J}^{m_j\neq m_k}\frac{1}{m_j - m_k}\left(N_{kj}\,\bar{Z}_{kj} + P_{kj}\,\bar{\psi}_{kj}\right)_{r_k}, \tag{A74}$$

$$B_{Ck} = -\frac{1}{r_k\,L_{0k}}\sum_{j=1,J}^{m_j\neq m_k}\frac{1}{m_j - m_k}\left(L_{kj}\,\bar{Z}_{kj} + M_{kj}\,\bar{\psi}_{kj}\right)_{r_k} + \frac{A_{Ck}}{L_{0k}}, \tag{A75}$$

$$\lambda_{Lk} = \frac{1}{2\,r_k}\left[\frac{P_{1k}\,L_{0k}}{\nu_{Lk}} + T_{1k} + \nu_{Lk}\left(\frac{L_{1k}}{L_{0k}} - 2\right)\right]_{r_k} - \frac{1}{(m_k\,s)_{r_k}}\frac{1}{r_k\,\nu_{Lk}}\sum_{j=1,J}^{m_j\neq m_k}\frac{1}{m_j - m_k}(P_{kj}\,L_{kj} - M_{kj}\,N_{kj})_{r_k}, \tag{A76}$$

$$\gamma_{Lk} = \frac{1}{2\,r_k}\left[(1 + \nu_{Lk})\left(\frac{P_{1k}}{\nu_{Lk}} + \frac{T_{1k}}{L_{0k}} - \frac{\nu_{Lk}}{L_{0k}}\right) + P_{0k}\left(\frac{L_{1k}}{L_{0k}} - 1\right)\right]_{r_k} - \frac{1}{(m_k\,s)_{r_k}}\frac{1}{r_k\,L_{0k}}\sum_{j=1,J}^{m_j\neq m_k}\frac{1}{m_j - m_k}(P_{kj}\,L_{kj} - M_{kj}\,N_{kj})_{r_k}, \tag{A77}$$

$$a_{kj} = -\frac{1}{(m_k\,s)_{r_k}}\left(\frac{M_{jk}}{\nu_{Lk}} + \frac{L_{jk}}{L_{0k}}\right)_{r_k}, \tag{A78}$$

$$b_{kj} = -\frac{1}{(m_k\,s)_{r_k}}\left(\frac{N_{jk}}{L_{0k}} + \frac{P_{jk}}{\nu_{Lk}}\right)_{r_k}, \tag{A79}$$

and

$$L_{1k} = \lim_{x\to 0}\left(\frac{L_{kk}}{m_k - n\,q}\right) - \frac{r_k\,L_{0k}}{x}, \tag{A80}$$

$$P_{1k} = \lim_{x\to 0}\left(\frac{P_{kk}}{m_k - n\,q}\right) - \frac{r_k\,P_{0k}}{x}, \tag{A81}$$

$$T_{1k} = \lim_{x\to 0}\left(\frac{-n\,q\,s}{m_k - n\,q}\right) - \frac{r_k}{x}. \tag{A82}$$

The parameters A_{Sk} and A_{Lk} are identified from the numerical solution of the outer equations in the vicinity of the rational surface by taking the limits

$$\bar{\psi}_{kj} = \psi_j(r_k+\delta) - a_{kj}\,\psi_k(r_k+\delta), \tag{A83}$$

$$\bar{Z}_{kj} = Z_j(r_k+\delta) - b_{kj}\,\psi_k(r_k+\delta), \tag{A84}$$

$$A^{\pm}_{Sk} = \pm\frac{Z_k(r_k\pm|\delta|) - b_{Lk}\,\psi_k(r_k\pm|\delta|)}{(b_{Sk}-b_{Lk})\,|\delta|^{\nu_{S\,k}}} - \frac{\left[(B_{Ck}-b_{Lk}\,A_{Ck}) + (\gamma_{Lk}-b_{Lk}\,\lambda_{Lk})\,\psi_k(r_k\pm|\delta|)\right]|\delta|}{(b_{Sk}-b_{Lk})\,|\delta|^{\nu_{S\,k}}}, \tag{A85}$$

$$A^{\pm}_{Lk} = \frac{\psi_k(r_k\pm|\delta|)\mp A^{\pm}_{Sk}|\delta|^{\nu_{S\,k}} \mp A_{Ck}\,|\delta|}{(1\pm|\delta|\,\lambda_{Lk})\,|\delta|^{\nu_{L\,k}}} \tag{A86}$$

as $|\delta|\to 0$. The previous analysis is based on the assumption that

$$-1 < D_{Ik} < 0. \tag{A87}$$

If $D_{Ik} > 0$, then the indices ν_{Lk} and ν_{Sk} become complex, indicating that the plasma in the vicinity of the kth rational surface is unstable to ideal interchange modes.[37] On the other hand, if $D_{Ik} < -1$, then the indices ν_{Lk} and ν_{Sk} differ by more than 2, and the expansion (A63)–(A66) must consequently be carried out to higher order in $|x|$.[38]

6. Asymptotic matching across the rational surface

Consider the resistive layer solution in the vicinity of the kth rational surface. This solution can be separated into independent tearing and twisting parity components.[26] The even (tearing parity) component is such that $\psi_k(-x) = \psi_k(x)$ throughout the layer, whereas the odd (twisting parity) component is such that $\psi_k(-x) = -\psi_k(x)$. It is helpful to define the quantities

$$A^e_{Lk} = \frac{1}{2}\left(A^+_{Lk} + A^-_{Lk}\right), \tag{A88}$$

$$A^o_{Lk} = \frac{1}{2}\left(A^+_{Lk} - A^-_{Lk}\right), \tag{A89}$$

$$A^e_{Sk} = \frac{1}{2}\left(A^+_{Sk} - A^-_{Sk}\right), \tag{A90}$$

$$A^o_{Sk} = \frac{1}{2}\left(A^+_{Sk} + A^-_{Sk}\right). \tag{A91}$$

The even and odd layer solutions determine the ratios[26]

$$\Delta^e_k = r_k^{\nu_{S\,k}-\nu_{L\,k}}\,\frac{2\,A^e_{Sk}}{A^e_{Lk}} \tag{A92}$$

and

$$\Delta^o_k = r_k^{\nu_{S\,k}-\nu_{L\,k}}\,\frac{2\,A^o_{Sk}}{A^o_{Lk}}, \tag{A93}$$

respectively. Moreover, the net toroidal electromagnetic torque acting on the layer can be shown to take the form[21,28]

$$\delta T_k = 2\,n\,\pi^2\left(\frac{\nu_{Sk}-\nu_{Lk}}{L_{kk}}\right)_{r_k}\left[|A^e_{Lk}|^2\,\mathrm{Im}\left(\Delta^e_k\right) + |A^o_{Lk}|^2\,\mathrm{Im}\left(\Delta^o_k\right)\right]. \tag{A94}$$

Let

$$\Psi^e_k = r_k^{\nu_{L\,k}}\left(\frac{\nu_{Sk}-\nu_{Lk}}{L_{kk}}\right)^{1/2}_{r_k} A^e_{Lk}, \tag{A95}$$

$$\Delta\Psi^e_k = r_k^{\nu_{S\,k}}\left(\frac{\nu_{Sk}-\nu_{Lk}}{L_{kk}}\right)^{1/2}_{r_k} 2\,A^e_{Sk}, \tag{A96}$$

$$\Psi^o_k = r_k^{\nu_{L\,k}}\left(\frac{\nu_{Sk}-\nu_{Lk}}{L_{kk}}\right)^{1/2}_{r_k} A^o_{Lk}, \tag{A97}$$

$$\Delta\Psi^o_k = r_k^{\nu_{S\,k}}\left(\frac{\nu_{Sk}-\nu_{Lk}}{L_{kk}}\right)^{1/2}_{r_k} 2\,A^o_{Sk}. \tag{A98}$$

The matching conditions become

$$\Delta\Psi^e_k = \Delta^e_k\;\Psi^e_k, \tag{A99}$$

$$\Delta\Psi^o_k = \Delta^o_k\;\Psi^o_k. \tag{A100}$$

Moreover,[21,28]

$$\delta T_k = 2\,n\,\pi^2\,\mathrm{Im}\left(\Psi^{e*}_k\,\Delta\Psi^e_k + \Psi^{o*}_k\,\Delta\Psi^o_k\right). \tag{A101}$$

7. Derivation of homogeneous dispersion relation

Let $\mathbf{y}(r)$ represent the $2J$-dimensional vector of the $\psi_j(r)$ and $Z_j(r)$ functions that satisfy the outer equations, (A47) and (A48).

Suppose that the plasma boundary corresponds to the flux-surface $r=b$ and that the plasma is surrounded by a perfectly conducting wall lying on the flux-surface $r=a$, where $a>b$. The region $b<r<a$ is a vacuum characterized by $g=1$ and $P=0$.

Let us launch J linearly independent, well-behaved solution vectors, $\mathbf{y}^e_j(r)$, for $j=1,J$, from the magnetic axis, $r=0$, and numerically integrate them to $r=a$. (It is generally necessary to periodically re-orthogonalize the solution vectors to prevent them from becoming co-linear. See Ref. 39, Appendix A 3.) The jump conditions imposed at the plasma rational surfaces are

$$\Psi^o_{k'} = 0, \tag{A102}$$

$$\Delta\Psi^e_{k'} = 0, \tag{A103}$$

for $k'=1,K$. Suppose that there are L rational surfaces lying in the vacuum region $b<r<a$. The jump conditions imposed at the vacuum rational surfaces are

$$\Psi^+_{l'} = \Psi^-_{l'}, \tag{A104}$$

$$\Delta\Psi^+_{l'} = \Delta\Psi^-_{l'}, \tag{A105}$$

for $l'=1,L$, where the $\Psi^{\pm}_{l'}$ and $\Delta\Psi^{\pm}_{l'}$ are defined in an analogous manner to the corresponding quantities for plasma rational surfaces (see Appendix A 5).

Next, let us launch a solution vector, $\Delta\mathbf{y}^e_k(r)$, from the kth plasma rational surface, and numerically integrate it to $r=a$. The jump conditions imposed at the plasma rational surfaces are

$$\Psi^o_{k'} = 0, \tag{A106}$$

$$\Delta\Psi^e_{k'} = \delta_{k'k}, \tag{A107}$$

for $k'=1,K$. The jump conditions (A104) and (A105) are again imposed at the vacuum rational surfaces.

We can form a linear combination of solution vectors,

$$\mathbf{Y}^e_k(r) = \sum_{j=1,J} \alpha^e_{jk}\,\mathbf{y}^e_j + \Delta\mathbf{y}^e_k, \tag{A108}$$

and choose the α^e_{jk} so as to ensure that the physical boundary condition

$$\psi_j(a) = 0, \tag{A109}$$

for $j=1,J$, is satisfied. By construction, this solution vector is such that

$$\Psi^o_{k'} = 0. \tag{A110}$$

$$\Delta\Psi^e_{k'} = \delta_{k'k}, \tag{A111}$$

for $k'=1,K$, and

$$\Psi^+_{l'} = \Psi^-_{l'}, \tag{A112}$$

$$\Delta\Psi^+_{l'} = \Delta\Psi^-_{l'}, \tag{A113}$$

for $l'=1,L$. Incidentally, the jump conditions (A112) and (A113) ensure that the solution vector is completely continuous across the vacuum rational surfaces, as must be the case in the absence of plasma currents. (Consequently, zero electromagnetic torque is exerted at these surfaces.) Let

$$\Psi^e_{k'} = F^{ee}_{k'k}, \tag{A114}$$

$$\Delta\Psi^o_{k'} = F^{oe}_{k'k}, \tag{A115}$$

for $k'=1,K$. We can associate a $\mathbf{Y}^e_k(r)$ with each rational surface in the plasma.

Let us launch J linearly independent, well-behaved solution vectors, $\mathbf{y}^o_j(r)$, for $j=1,J$, from the magnetic axis, $r=0$, and numerically integrate them to $r=a$. The jump conditions imposed at the plasma rational surfaces are

$$\Psi^e_{k'} = 0, \tag{A116}$$

$$\Delta\Psi^o_{k'} = 0, \tag{A117}$$

for $k'=1,K$. The jump conditions (A104) and (A105) are again imposed at the vacuum rational surfaces.

Next, we can launch a solution vector, $\Delta\mathbf{y}^o_k(r)$, from the kth rational surface, and integrate it to $r=a$. The jump conditions imposed at the plasma rational surfaces are

$$\Psi^e_{k'} = 0, \tag{A118}$$

$$\Delta\Psi^o_{k'} = \delta_{k'k}, \tag{A119}$$

for $k=1,K$. As before, the jump conditions (A104) and (A105) are imposed at the vacuum rational surfaces.

We can form the linear combination of solution vectors,

$$\mathbf{Y}^o_k(r) = \sum_{j=1,J} \alpha^o_{jk}\,\mathbf{y}^o_j + \Delta\mathbf{y}^o_k, \tag{A120}$$

and choose the α^o_{jk} so as to satisfy the boundary condition (A109). By construction, this solution vector is such that

$$\Psi^e_{k'} = 0, \tag{A121}$$

$$\Delta\Psi^o_{k'} = \delta_{k'k}, \tag{A122}$$

for $k'=1,K$, and

$$\Psi^+_{l'} = \Psi^-_{l'}, \tag{A123}$$

$$\Delta\Psi^+_{l'} = \Psi^-_{l'}, \tag{A124}$$

for $l'=1,L$. Let

$$\Psi^o_{k'} = F^{oo}_{k'k}, \tag{A125}$$

$$\Delta\Psi^e_{k'} = F^{eo}_{k'k}, \tag{A126}$$

for $k'=1,K$. We can associate a $\mathbf{Y}^o_k(r)$ with each rational surface in the plasma.

The most general well-behaved solution vector that satisfies the boundary condition (A109) is written as

$$\mathbf{Y}(r) = \sum_{k=1,K} \left(a_k\,\mathbf{Y}^e_k + b_k\,\mathbf{Y}^o_k\right), \tag{A127}$$

where the a_k and b_k are arbitrary. It follows that

$$\Psi^e_k = \sum_{k'=1,K} F^{ee}_{kk'}\,a_{k'}, \tag{A128}$$

$$\Psi^o_k = \sum_{k'=1,K} F^{oo}_{kk'}\,b_{k'}, \tag{A129}$$

$$\Delta\Psi^e_k = a_k + \sum_{k'=1,K} F^{eo}_{kk'}\,b_{k'}, \tag{A130}$$

$$\Delta\Psi^o_k = b_k + \sum_{k'=1,K} F^{oe}_{kk'}\,a_{k'}, \tag{A131}$$

for $k=1,K$. Let $\boldsymbol{\Psi}^e$, $\boldsymbol{\Psi}^o$, $\Delta\boldsymbol{\Psi}^e$, and $\Delta\boldsymbol{\Psi}^o$ be the $K\times 1$ vectors of the Ψ^e_k, Ψ^o_k, $\Delta\Psi^e_k$, and $\Delta\Psi^o_k$ values, respectively. Let $\mathbf{F}^{ee}$, $\mathbf{F}^{eo}$, $\mathbf{F}^{oe}$, and $\mathbf{F}^{oo}$ be the $K\times K$ matrices of the $F^{ee}_{kk'}$, $F^{eo}_{kk'}$, $F^{oe}_{kk'}$, and $F^{oo}_{kk'}$ values, respectively. Equations (A128)–(A131) can be combined to give the dispersion relation

$$\begin{pmatrix} \Delta\boldsymbol{\Psi}^e \\ \Delta\boldsymbol{\Psi}^o \end{pmatrix} = \begin{pmatrix} \mathbf{E}^e & \boldsymbol{\Gamma} \\ \boldsymbol{\Gamma}' & \mathbf{E}^o \end{pmatrix} \begin{pmatrix} \boldsymbol{\Psi}^e \\ \boldsymbol{\Psi}^o \end{pmatrix}, \tag{A132}$$

where

$$\mathbf{E}^e = (\mathbf{F}^{ee})^{-1}, \tag{A133}$$

$$\mathbf{E}^o = (\mathbf{F}^{oo})^{-1}, \tag{A134}$$

$$\boldsymbol{\Gamma} = \mathbf{F}^{eo}\,\mathbf{E}^o, \tag{A135}$$

$$\boldsymbol{\Gamma}' = \mathbf{F}^{oe}\,\mathbf{E}^e. \tag{A136}$$

Now, according to Eqs. (A61) and (A109),

$$T_\phi(a) = \sum_{k=1,K} \delta T_k = 0. \tag{A137}$$

In other words, the net toroidal electromagnetic torque acting on the plasma is zero. Hence, Eq. (A101) yields

$$\boldsymbol{\Psi}^{e\dagger}\,\Delta\boldsymbol{\Psi}^e - \Delta\boldsymbol{\Psi}^{e\dagger}\,\boldsymbol{\Psi}^e + \boldsymbol{\Psi}^{o\dagger}\,\Delta\boldsymbol{\Psi}^o - \Delta\boldsymbol{\Psi}^{o\dagger}\,\boldsymbol{\Psi}^o = 0. \tag{A138}$$

Thus, making use of the dispersion relation (A132), we deduce that[20–22,28]

$$\mathbf{E}^{e\dagger} = \mathbf{E}^e, \tag{A139}$$

$$\mathbf{E}^{o\dagger} = \mathbf{E}^o, \tag{A140}$$

$$\boldsymbol{\Gamma}' = \boldsymbol{\Gamma}^\dagger. \tag{A141}$$

Hence, the homogeneous dispersion relation can be written as[20,22,27,28]

$$\begin{pmatrix} \mathbf{E}^e - \Delta^e & \boldsymbol{\Gamma} \\ \boldsymbol{\Gamma}' & \mathbf{E}^o - \Delta^o \end{pmatrix} \begin{pmatrix} \boldsymbol{\Psi}^e \\ \boldsymbol{\Psi}^o \end{pmatrix} = \begin{pmatrix} 0 \\ 0 \end{pmatrix}, \tag{A142}$$

where Δ^e and Δ^o are the diagonal $K\times K$ matrices of the Δ^e_k and Δ^o_k values, respectively. Note that, according to Eqs. (A139)–(A141), the $\mathbf{E}^e$ and $\mathbf{E}^o$ matrices are Hermitian, and the $\boldsymbol{\Gamma}'$ matrix is the Hermitian conjugate of the $\boldsymbol{\Gamma}$ matrix.

8. Derivation of inhomogeneous dispersion relation

Let us define the solution vectors

$$\tilde{\mathbf{Y}}^e_k(r) = \sum_{k''=1,K} E^e_{k''k}\,\mathbf{Y}^e_{k''}, \tag{A143}$$

for $k = 1,K$. It follows, from Appendix A 7, that these vectors are well-behaved solutions of the outer equations, satisfying the physical boundary condition at the wall, and having the properties that

$$\Psi^e_{k'} = \delta_{k'k}, \tag{A144}$$

$$\Psi^o_{k'} = 0, \tag{A145}$$

$$\Delta\Psi^e_{k'} = E^e_{k'k}, \tag{A146}$$

$$\Delta\Psi^o_{k'} = \Gamma^*_{kk'}, \tag{A147}$$

for $k' = 1,K$. Let the $\tilde{\psi}^e_{k,j}(r)$ and the $\tilde{Z}^e_{k,j}(r)$ be the elements of the $\tilde{\mathbf{Y}}^e_k(r)$ solution vector, for $j = 1,J$. By construction, we have

$$\tilde{\psi}^e_{k,j}(a) = 0, \tag{A148}$$

for $j = 1,J$.

Let us define the solution vectors

$$\tilde{\mathbf{Y}}^o_k(r) = \sum_{k''=1,K} E^o_{k''k}\,\mathbf{Y}^o_{k''}, \tag{A149}$$

for $k = 1,K$. It follows, from Appendix A 7, that these vectors are well-behaved solutions of the outer equations, satisfying the physical boundary condition at the wall, and having the properties that

$$\Psi^e_{k'} = 0, \tag{A150}$$

$$\Psi^o_{k'} = \delta_{k'k}, \tag{A151}$$

$$\Delta\Psi^e_{k'} = \Gamma_{k'k}, \tag{A152}$$

$$\Delta\Psi^o_{k'} = E^o_{k'k}, \tag{A153}$$

for $k' = 1,K$. Let the $\tilde{\psi}^o_{k,j}(r)$ and the $\tilde{Z}^o_{k,j}(r)$ be the elements of the $\tilde{\mathbf{Y}}^o_k(r)$ solution vector, for $j = 1,J$. By construction, we have

$$\tilde{\psi}^o_{k,j}(a) = 0, \tag{A154}$$

for $j = 1,J$.

The most general well-behaved solution vector in the presence of an external magnetic perturbation is written as

$$\mathbf{Y}(r) = \sum_{k=1,K} \left(\Psi^e_k\,\tilde{\mathbf{Y}}^e_k + \Psi^o_k\,\tilde{\mathbf{Y}}^o_k\right) + \mathbf{Y}^x, \tag{A155}$$

where $\mathbf{Y}^x(r)$ is the solution vector that describes the ideal (i.e., $\Psi^e_k = \Psi^o_k = 0$ for $k = 1,K$) response of the plasma to the perturbation. This solution vector is characterized by

$$\Psi^e_{k'} = 0, \tag{A156}$$

$$\Psi^o_{k'} = 0, \tag{A157}$$

$$\Delta\Psi^e_{k'} = -\chi^e_{k'}, \tag{A158}$$

$$\Delta\Psi^o_{k'} = -\chi^o_{k'}, \tag{A159}$$

for $k' = 0,K$. Thus, in the presence of the external perturbation, the homogenous dispersion relation (A132) generalizes to the inhomogenous relation

$$\begin{pmatrix} \mathbf{E}^e - \Delta^e & \boldsymbol{\Gamma} \\ \boldsymbol{\Gamma}' & \mathbf{E}^o - \Delta^o \end{pmatrix} \begin{pmatrix} \boldsymbol{\Psi}^e \\ \boldsymbol{\Psi}^o \end{pmatrix} = \begin{pmatrix} \boldsymbol{\chi}^e \\ \boldsymbol{\chi}^o \end{pmatrix}, \tag{A160}$$

where $\boldsymbol{\chi}^e$ and $\boldsymbol{\chi}^o$ are the $K\times 1$ vectors of the χ^e_k and χ^O_k values, respectively.

Let the $\psi^x_j(r)$ and the $Z^x_j(r)$ be the elements of the $\mathbf{Y}^x(r)$ solution vector, for $j = 1,J$. Suppose that

$$\psi^x_j(a) = \frac{a}{q(a)}\left[m_j - n\,q(a)\right]\Xi_j, \tag{A161}$$

$$Z^x_j(a) = \Omega_j, \tag{A162}$$

for $j = 1,J$. According to Eq. (A61), the net toroidal electromagnetic torque acting on the plasma is written as

$$T_\phi(a) = \sum_{k=1,K} \delta T_k = -2\,n\,\pi^2\,\mathrm{Im}\sum_{j=1,J} \frac{Z^*_j\,\psi_j}{m_j - n\,q}\bigg|_{r=a}. \tag{A163}$$

However,

$$\psi_j(a) = \frac{a}{q(a)}\left[m_j - n\,q(a)\right]\Xi_j, \tag{A164}$$

$$Z_j(a) = \sum_{k=1,K}\left[\Psi^e_k\,\tilde{Z}^e_{k,j}(a) + \Psi^o_k\,\tilde{Z}^o_{k,j}(a)\right] + \Omega_j, \tag{A165}$$

so

$$T_\phi(a) = -2\,n\,\pi^2\,\mathrm{Im}\sum_{J=1,J}\sum_{k=1,K}\frac{a}{q(a)}\,\Xi_j \times\left[\Psi^e_k\,\tilde{Z}^e_{k,j}(a)+\Psi^o_k\,\tilde{Z}^o_{k,j}(a)\right]^*. \tag{A166}$$

Here, we have assumed that

$$\mathrm{Im}\sum_{j=1,J}\Omega^*_j\,\Xi_j = 0; \tag{A167}$$

otherwise, the external perturbation would be able to exert a torque on an ideal plasma (i.e., a plasma in which $\Psi^e_k = \Psi^o_k = 0$, for $k = 1, K$), which is unphysical.

It follows from Eqs. (A101) and (A160), as well as the fact that $\mathbf{E}^e$ and $\mathbf{E}^o$ matrices are Hermitian, that

$$T_\phi(a) = \sum_{k=1,K}\delta T_k = -2\,n\,\pi^2\,\mathrm{Im}\sum_{k=1,K}\left(\Psi^{e*}_k\,\chi^e_k+\Psi^{o*}_k\,\chi^o_k\right). \tag{A168}$$

Comparison with Eq. (A166) reveals that

$$\chi^e_k = \sum_{j=1,J}\xi^{e*}_{k,j}\,\Xi_j, \tag{A169}$$

$$\chi^o_k = \sum_{j=1,J}\xi^{o*}_{k,j}\,\Xi_j, \tag{A170}$$

where

$$\xi^e_{k,j} = \frac{a}{q(a)}\,\tilde{Z}^e_{k,j}(a), \tag{A171}$$

$$\xi^o_{k,j} = \frac{a}{q(a)}\,\tilde{Z}^o_{k,j}(a). \tag{A172}$$

APPENDIX B: SOLUTION OF LINEARIZED RESISTIVE-MHD LAYER EQUATIONS

1. Basic equations

Let us assume that all perturbed quantities vary in time as $\exp(\gamma\,t)$, where γ is the complex growth-rate of the instability. The linearized, resistive-MHD equations that govern perturbed quantities in the inner region are[26]

$$\delta\mathbf{B} = \nabla\times(\boldsymbol{\xi}\times\mathbf{B}) - \frac{\eta}{\gamma'}\,\nabla\times\delta\mathbf{J}, \tag{B1}$$

$$\nabla\delta P = \delta\mathbf{J}\times\mathbf{B}+\mathbf{J}\times\delta\mathbf{B}-\rho\,\gamma'^2\,\boldsymbol{\xi}, \tag{B2}$$

$$\delta\mathbf{J} = \nabla\times\delta\mathbf{B}, \tag{B3}$$

$$\delta P = -\boldsymbol{\xi}\cdot\nabla P - \Gamma\,P\,\nabla\cdot\boldsymbol{\xi}. \tag{B4}$$

Here,

$$\gamma'(r) = \gamma - \mathrm{i}\,n\,\Omega_\phi(r), \tag{B5}$$

where $\Omega_\phi(r)$ is the plasma toroidal angular velocity. (We are neglecting the effect of velocity shear in the preceding equations.) Moreover, $\eta(r)$ and $\rho(r)$ are the plasma resistivity and density profiles, respectively. Finally, $\Gamma = 5/3$ is the plasma ratio of specific heats.

2. Layer equations

Consider the segment of the inner region centered on the kth rational surface. It is helpful to define

$$a_0(r) = \langle R^2\rangle, \tag{B6}$$

$$c_0(r) = \langle|\nabla r|^{-2}\rangle, \tag{B7}$$

$$d_0(r) = \langle|\nabla r|^{-2}\,R^2\rangle, \tag{B8}$$

$$e_0(r) = \langle|\nabla r|^{-2}\,R^4\rangle, \tag{B9}$$

$$x_0(r) = \langle|\nabla r|^2\rangle, \tag{B10}$$

$$y_0(r) = \langle R^4\rangle, \tag{B11}$$

as well as

$$F_R(r) = \frac{1+x_0\,\alpha_\epsilon/q^2}{c_0+\alpha_\epsilon/q^2}, \tag{B12}$$

$$F_A(r) = \frac{y_0\left(1+x_0\,\alpha_\epsilon/q^2\right)-a_0^2}{f^2\,F_R}, \tag{B13}$$

and

$$\omega_H(r) = \frac{B_0}{R_0}\,\frac{n\,s}{\sqrt{\mu_0\,\rho\,F_A}}, \tag{B14}$$

$$\omega_\eta(r) = \frac{\eta\,F_R}{\mu_0\,R_0^2\,r^2}, \tag{B15}$$

$$L(r) = \frac{\omega_H}{\omega_\eta}. \tag{B16}$$

It is assumed that $L \gg 1$. Here, $\langle\cdots\rangle = \oint(\cdots)\,d\theta/2\pi$ is a flux-surface average operator.

In the vicinity of the kth rational surface, Eqs. (B1)–(B4) can be shown to reduce to[26]

$$0 = \frac{d^2\Psi}{dX^2} - H_k\,\frac{d\Upsilon}{dX} - Q_k\,(\Psi - X\,\Xi), \tag{B17}$$

$$0 = Q_k^2\,\frac{d^2\Xi}{dX^2} - Q_k\,X^2\,\Xi + E_k\,\Upsilon + Q_k\,X\,\Psi + \Lambda, \tag{B18}$$

$$0 = Q_k\,\frac{d^2\Upsilon}{dX^2} - X^2\,\Upsilon - G_k\,Q_k^2\,\Upsilon + (G_k - K_k\,E_k)\,Q_k^2\,\Xi + X\,\Psi - K_k\,Q_k^2\,\Lambda, \tag{B19}$$

$$0 = H_k\,\frac{d^2\Lambda}{dX^2} - \frac{d\Lambda}{dX} + F_k\,\frac{d\Upsilon}{dX}. \tag{B20}$$

Here,

$$x = r - r_k, \tag{B21}$$

$$\Psi(x) = \psi_k(x), \tag{B22}$$

$$X = \left(L^{1/3}\,\frac{x}{r}\right)_{r_k}, \tag{B23}$$

$$Q_k = \left(L^{1/3}\,\frac{\gamma'}{\omega_H}\right)_{r_k}, \tag{B24}$$

and

$$E_k = \left[\frac{\alpha_p}{s^2}\left\{\left(c_0+\alpha_\epsilon/q^2\right)\left(-r\frac{da_0}{dr}+a_0\,\alpha_f\right)+\frac{a_0\,s}{F_R}\right\}\right]_{r_k}, \tag{B25}$$

$$F_k = \left[\frac{\alpha_p^2}{s^2}\left(\left[c_0+\alpha_\epsilon/q^2\right]e_0-d_0^2\right)\right]_{r_k}, \tag{B26}$$

$$G_k = \left[\frac{a_0\left(c_0+\alpha_\epsilon/q^2\right)}{\Gamma P}\frac{F_R}{F_A}\right]_{r_k}, \tag{B27}$$

$$H_k = \left[\frac{\alpha_p}{s}\left(d_0-\frac{a_0}{F_R}\right)\right]_{r_k}, \tag{B28}$$

$$K_k = \left[\frac{s^2}{\alpha_p^2 f^2}\frac{F_R}{F_A}\right]_{r_k}. \tag{B29}$$

Let us write

$$\Psi(X) = \Psi^e(X)+\Psi^o(X)+A_0\,X, \tag{B30}$$

$$\Xi(X) = \Xi^e(X)+\Xi^o(X)+A_0, \tag{B31}$$

$$\Upsilon(X) = \Upsilon^e(X)+\Upsilon^o(X)+A_0, \tag{B32}$$

$$\Lambda(X) = \Lambda^e(X)+\Lambda^o(X)-A_0\,E_k, \tag{B33}$$

where A_0 is an arbitrary constant, and $\Psi^e(-X)=\Psi^e(X)$, $\Psi^o(-X)=-\Psi^o(X)$, etc. Equations (B17)–(B20) can be shown to separate into the following two independent sets of equations:[26]

$$0 = \frac{d^2\Psi^{e,o}}{dX^2}-H_k\frac{d\Upsilon^{o,e}}{dX}-Q_k\left(\Psi^{e,o}-X\,\Xi^{o,e}\right), \tag{B34}$$

$$0 = Q_k^2\frac{d^2\Xi^{o,e}}{dX^2}-Q_k\,X^2\,\Xi^{o,e}+\left(E_k+F_k\right)\Upsilon^{o,e} + Q_k\,X\,\Psi^{e,o}+H_k\frac{d\Psi^{e,o}}{dX}, \tag{B35}$$

$$0 = Q_k\frac{d^2\Upsilon^{o,e}}{dX^2}-X^2\,\Upsilon^{o,e}-Q_k^2\left(K_k\,F_k+G_k\right)\Upsilon^{o,e} + Q_k^2\left(G_k-K_k\,E_k\right)\Xi^{o,e}-Q_k^2\,K_k\,H_k\frac{d\Psi^{e,o}}{dX}, \tag{B36}$$

where

$$\Lambda^{o,e} = H_k\frac{d\Psi^{e,o}}{dX}+F_k\,\Upsilon^{o,e}. \tag{B37}$$

The first set (involving Ψ^e) governs tearing parity layer solutions, whereas the second (involving Ψ^o) governs twisting parity solutions.

3. Asymptotic matching

In the limit $|X|\rightarrow\infty$, the asymptotic behavior of the well-behaved solutions of the layer equations, (B34)–(B37), is such that

$$\Psi^e(X)\rightarrow a_L^e\,|X|^{\nu_{L\,k}}+a_S^e\,|X|^{\nu_{S\,k}}, \tag{B38}$$

$$\Psi^o(X)\rightarrow \mathrm{sgn}(X)\left(a_L^o\,|X|^{\nu_{L\,k}}+a_S^o\,|X|^{\nu_{S\,k}}\right). \tag{B39}$$

These solutions are undetermined to an arbitrary multiplicative constant, which means that the ratios a_S^e/a_L^e and a_S^o/a_L^o are fully determined. Here,

$$\nu_{Lk} = \frac{1}{2}-\sqrt{-D_{Ik}}, \tag{B40}$$

$$\nu_{Sk} = \frac{1}{2}+\sqrt{-D_{Ik}}, \tag{B41}$$

where

$$D_{Ik} = E_k+F_k+H_k-\frac{1}{4}. \tag{B42}$$

The parameter D_{Ik} can be shown to be identical to the corresponding parameter defined in Appendix A 5. Asymptotic matching to the ideal-MHD solution in the outer region yields

$$\Delta_k^e = L_k^{(\nu_{S\,k}-\nu_{L\,k})/3}\,\hat{\Delta}_k^e, \tag{B43}$$

$$\Delta_k^o = L_k^{(\nu_{S\,k}-\nu_{L\,k})/3}\,\hat{\Delta}_k^o, \tag{B44}$$

where $L_k = L(r_k)$, and

$$\hat{\Delta}_k^e = \frac{2\,a_S^e}{a_L^e}, \tag{B45}$$

$$\hat{\Delta}_k^o = \frac{2\,a_S^o}{a_L^o}. \tag{B46}$$

The hydromagnetic frequency, resistive diffusion rate, and Lundquist number of the plasma are defined as

$$\omega_A(r) = \frac{B_0}{R_0}\frac{1}{\sqrt{\mu_0\,\rho}}, \tag{B47}$$

$$\omega_R(r) = \frac{\eta}{\mu_0\,R_0^2\,\bar{a}^2}, \tag{B48}$$

$$S(r) = \frac{\omega_A}{\omega_R}, \tag{B49}$$

respectively. Here, the plasma minor radius, $\bar{a}$, is specified in Sec. V. It follows that

$$S = f_S\,L, \tag{B50}$$

$$\omega_A = f_A\,\omega_H, \tag{B51}$$

where

$$f_S(r) = \frac{F_A^{1/2}\,F_R}{n\,s}\frac{\bar{a}^2}{r^2}, \tag{B52}$$

$$f_A(r) = \frac{F_A^{1/2}}{n\,s}. \tag{B53}$$

Thus, we can write

$$\Delta_k^e = (S_k)^{(2/3)\sqrt{-D_{I\,k}}}\,\tilde{\Delta}_k^e\left(\tilde{Q}_k, E_k+F_k, H_k, K_k\,E_k - G_k, K_k\,F_k+G_k, K_k\,H_k, f_{Ak}, f_{Sk}\right), \tag{B54}$$

$$\Delta_k^o = (S_k)^{(2/3)\sqrt{-D_{I\,k}}}\,\tilde{\Delta}_k^o\left(\tilde{Q}_k, E_k+F_k, H_k, K_k\,E_k - G_k, K_k\,F_k+G_k, K_k\,H_k, f_{Ak}, f_{Sk}\right), \tag{B55}$$

where

$$\gamma = \mathrm{i}\,n\,\Omega_k+\frac{\tilde{Q}_k}{(S_k)^{1/3}}\,\omega_{Ak}, \tag{B56}$$

and

$$\tilde{Q}_k = \left(\frac{f_{Sk}^{1/3}}{f_{Ak}}\right) Q_k, \tag{B57}$$

$$\tilde{\Delta}_k^{e,o} = \frac{\hat{\Delta}_k^{e,o}}{f_{Sk}^{(2/3)\sqrt{-D_{I\,k}}}}. \tag{B58}$$

Here, $S_k = S(r_k)$, $\Omega_k = \Omega(r_k)$, $\omega_{Ak} = \omega_A(r_k)$, $f_{Ak} = f_A(r_k)$, and $f_{Sk} = f_S(r_k)$.

[1]R. Fitzpatrick, Phys. Plasmas **5**, 3325 (1998).
[2]Z. Chang and J. D. Callen, Nucl. Fusion **30**, 219 (1990).
[3]J. T. Scoville, R. J. La Haye, A. G. Kellman, T. H. Osbourne, R. D. Stambaugh, E. J. Strait, and T. S. Taylor, Nucl. Fusion **31**, 875 (1991).
[4]T. C. Hender, R. Fitzpatrick, A. W. Morris, P. G. Carolan, R. D. Durst, T. Edlington, J. Ferreira, S. J. Fielding, P. S. Haynes, J. Hugill, I. J. Jenkins, R. J. La Haye, B. J. Parham, D. C. Robinson, T. N. Todd, M. Valovič, and G. Vayakis, Nucl. Fusion **32**, 2091 (1992).
[5]G. M. Fishpool and P. S. Haynes, Nucl. Fusion **34**, 109 (1994).
[6]R. J. Buttery, M. De Benedetti, D. A. Gates, Y. Gribov, T. C. Hender, R. J. La Haye, P. Leahy, J. A. Leuer, A. W. Morris, A. Santagiustina, J. T. Scoville, B. J. D. Tubbing, JET Team, COMPASS-D Research Team, and DIII-D Team. Nucl. Fusion **39**, 1827 (1999).
[7]R. J. Buttery, M. De Benedetti, T. C. Hender, and B. J. D. Tubbing, Nucl. Fusion **40**, 807 (2000).
[8]S. M. Wolfe, I. R. Hutchinson, R. S. Granetz, J. Rice, A. Hubbard, A. Lynn, P. Phillips, T. C. Hender, D. F. Howell, R. J. La Haye, and J. T. Scoville, Phys. Plasmas **12**, 056110 (2005).
[9]H. Reimerdes, J. Bialek, M. S. Chance, M. S. Chu, A. M. Garofalo, P. Gohil, Y. In, G. L. Jackson, R. J. Jayakumar, T. H. Jensen, J. S. Kim, R. J. La Haye, Y. Q. Liu, J. E. Menard, G. A. Navratil, M. Okabayashi, J. T. Scoville, E. J. Strait, D. D. Szymanski, and H. Takahashi, Nucl. Fusion **45**, 368 (2005).
[10]H. Reimerdes, T. C. Hender, S. A. Sabbagh, J. M. Bialek, M. S. Chu, A. M. Garofalo, M. P. Gryaznevich, D. F. Howell, G. L. Jackson, R. J. La Haye, Y. Q. Liu, J. E. Menard, G. A. Navratil, M. Okabayashi, S. D. Pinches, A. C. Sontag, E. J. Strait, W. Zhu, M. Bigi, M. de Baar, P. de Vries, D. A. Gates, P. Gohil, R. J. Groebner, D. Mueller, R. Raman, J. T. Scoville, W. M. Solomon, DIII-D Team, JET-EFDA Contributors, and NSTX Team Phys. Plasmas **13**, 056107 (2006).
[11]M. P. Gryaznevich, T. C. Hender, D. F. Howell, C. D. Challis, H. R. Koslowski, S. Gerasimov, E. Joffrin, Y. Q. Liu, S. Saarelma, and JET-EFDA Contributers, Plasma Phys. Controlled Fusion **50**, 124030 (2008).
[12]R. Fitzpatrick, Plasma Phys. Controlled Fusion **54**, 094002 (2012).
[13]Y. Liu, J. W. Connor, S. C. Cowley, C. J. Ham, R. J. Hastie, and T. C. Hender, Phys. Plasmas **19**, 072509 (2012).
[14]ITER Physics Basis Editors, Nucl. Fusion **39**, 2175 (1999).
[15]J. K. Park, M. Schaffer, J. E. Menard, and A. H. Boozer, Phys. Rev. Lett. **99**, 195003 (2007).
[16]Y. Liu, A. Kirk, and Y. Sun, Phys. Plasmas **20**, 042503 (2013).
[17]N. M. Ferraro, T. E. Evans, L. L. Lao, R. A. Moyer, R. Nazikian, D. M. Orlov, M. W. Schaffer, E. A. Unterberg, M. R. Wade, and A. Wingen, Nucl. Fusion **53**, 073042 (2013).
[18]J. K. Park, A. H. Boozer, and A. H. Glasser, Phys. Plasmas **14**, 052110 (2007).
[19]J. W. Connor, S. C. Cowley, R. J. Hastie, T. C. Hender, A. Hood, and T. J. Martin, Phys. Fluids **31**, 577 (1988).
[20]A. Pletzer and R. L. Dewar, J. Plasma Phys. **45**, 427 (1991).
[21]R. Fitzpatrick, R. J. Hastie, T. J. Martin, and C. M. Roach, Nucl. Fusion **33**, 1533 (1993).
[22]R. L. Dewar and M. Persson, Phys. Fluids B **5**, 4273 (1993).
[23]A. Pletzer, A. Bondeson, and R. L. Dewar, J. Comput. Phys. **115**, 530 (1994).
[24]A. H. Glasser, Z. R. Wang, and J.-K. Park, Phys. Plasmas **23**, 112506 (2016).
[25]H. P. Furth, J. Killeen, and M. N. Rosenbluth, Phys. Fluids **6**, 459 (1963).
[26]A. H. Glasser, J. M. Greene, and J. L. Johnson, Phys. Fluids **18**, 875 (1975).
[27]J. W. Connor, R. J. Hastie, and J. B. Taylor, Phys. Fluids B **3**, 1539 (1991).
[28]R. Fitzpatrick, Phys. Plasmas **1**, 3308 (1994).
[29]A. H. Glasser, S. C. Jardin, and G. Tesauro, Phys. Fluids **27**, 1225 (1984).
[30]H. Lütjens, A. Bondeson, and O. Sauter, Comput. Phys. Commun. **97**, 219 (1996).
[31]P. H. Rebut, R. J. Bickerton, and B. E. Keen, Nucl. Fusion **25**, 1011 (1985).
[32]J. K. Park, A. H. Boozer, J. E. Menard, and M. J. Schaffer, Nucl. Fusion **48**, 045006 (2008).
[33]R. Fitzpatrick, Phys. Plasmas **22**, 042514 (2015).
[34]D. P. Brennan, R. J. La Haye, A. D. Turnbull, M. S. Chu, T. H. Jensen, L. L. Lao, T. C. Luce, P. A. Politzer, E. J. Strait, S. E. Kruger, and D. D. Schnack, Phys. Plasmas **10**, 1643 (2003).
[35]M. Kotschenreuther, R. D. Hazeltine, and P. J. Morrison, Phys. Fluids **28**, 294 (1985).
[36]R. Carrera, R. D. Hazeltine, and M. Kotschenreuther, Phys. Fluids **29**, 899 (1986).
[37]C. Mercier, Nucl. Fusion **1**, 47 (1960).
[38]A. H. Glasser, Phys. Plasmas **23**, 072505 (2016).
[39]C. J. Ham, J. W. Connor, S. C. Cowley, C. G. Gimblett, R. J. Hastie, T. C. Hender, and T. J. Martin, Plasma Phys. Controlled Fusion **54**, 025009 (2012).